LUND UNIVERSITY

Chloride ion dynamics in neuronal homeostasis and plasticity: Measuring a zero current with a twitch of learning

Fåhraeus, Christer

2019

Document Version:
Förlagets slutgiltiga version

[Link to publication](#)

Citation for published version (APA):
Fåhraeus, C. (2019). *Chloride ion dynamics in neuronal homeostasis and plasticity: Measuring a zero current with a twitch of learning.* Lund University: Faculty of Medicine.

Total number of authors:
1

Chloride ion dynamics in neuronal homeostasis and plasticity

Measuring a zero current with a twitch of learning

Christer Fåhræus

LUND
UNIVERSITY

ACADEMIC DISSERTATION

by due permission of the Faculty of Medicine, Lund University, Sweden.
To be defended on the 12th of January 2019, at 09:00,
in Belfragesalen, BMC D15, Klinikgatan 32, Lund.

Faculty opponent

Professor Boris Barbour
École Normale Supérieure
Paris, France

Organization	Document name
LUND UNIVERSITY Neural Basis of Sensorimotor Control Neurophysiology & Neuronano Department of Experimental Medical Science BMC 221 84, Lund, Sweden	DOCTORAL DISSERTATION
	Date of issue 12th of January, 2019
Author: Christer Fåhræus	Sponsoring organization

Title and subtitle
Chloride ion dynamics in neuronal homeostasis and plasticity: Measuring a zero current with a twitch of learning

Abstract

Chloride is the most abundant physiological anion in animal cells. Yet, the importance of chloride ions in neurons has not been fully recognized until recently. Today not only synaptic inhibition is critically associated with Cl^- gradients but also synaptic plasticity, learning and cell volume control. In order to analyze the Cl^- homeostasis in a neuron, quantification of the Cl^- leakage from intracellular microelectrodes was needed. In Paper I the electrical and biophysical characteristics of KCl filled microelectrodes were investigated. For the first time, the fluxes of Cl^- from a microelectrode, during passive and active current injection, could be quantitatively determined. Based on these measurements, a comprehensive mathematical microelectrode model was derived (Paper II). It was shown that the model could reproduce all experimental data and predict classical properties such as tip potential, current rectification and electrode resistance but also predict data on the leakage of K^+ and Cl^- during intracellular microelectrode work.

In Paper III and IV, investigating the transmembrane turnover of Cl^- in a neuron, a powerful K-Cl cotransporter was identified, responsible for keeping intracellular Cl^- concentration low, thus enabling efficient GABAergic inhibition. Further, by combining data on the known ion channels and the microelectrode, a quantitative model of the K-Cl cotransporter could be deduced, for the first time in a neuron. From neuronal model simulations it was concluded that the cotransporter is probably also important in diminishing extracellular K^+ increases, thereby avoiding spreading depression phenomena in the CNS.

In conclusion, chloride ions are pivotal not only for a functional inhibitory system and the level of excitability in the CNS, but also in learning, plasticity and neuronal network maturation. The present work can help understanding the important interplay between the K-Cl cotransporter and intracellular Cl^- with potential long-term implications for how to deploy disease modifying drugs in neuropathologies.

Key words: K-Cl cotransporter, Cl^- homeostasis, DIDS, SITS, bumetanide, mathematical modeling, intracellular glass microelectrode, electrodiffusion, electro-osmosis, tip potential, Hebb, learning

Classification system and/or index terms (if any)

Supplementary bibliographical information		Language: Eng (Swe)
ISSN and key title 1652-8220		ISBN 978-91-7619-731-8
Recipient's notes	Number of pages: 86	Price: Free
	Security classification: Official	

Chloride ion dynamics in neuronal homeostasis and plasticity

Measuring a zero current with a twitch of learning

Christer Fåhræus

To my family and friends

Table of Contents

Foreword

When I began my doctoral studies in the Department of Physiology at the Medical Faculty of Lund University, it was to explore the last frontier of science, as I remember calling it. Neuroscience was a field where so much obvious ingenuity, efficiency and marvel was easy to observe, but the knowledge to explain it, was hidden in darkness. For me the answer was obvious – computational neuroscience was the discipline that would change this - and engineers rather than doctors would solve the puzzle. My background, with the equivalent of five years studies almost exclusively in math and physics, plus three years in med school, made me feel confidently up to the task. The grand plan was to start with perfecting a realistic mathematical model of the stretch receptor neuron with the late Prof Wolfgang Grampp's group and then apply this, more detailed, neuron model to make even more realistic simulations of neural networks. In the next step, I would start to investigate the truly exciting parts of neuroscience such as plasticity, memory formation and learning mechanisms.

As part of this plan I got a scholarship to pursue a Graduate degree at University of California. The choice fell on UC San Diego, the birthplace of Parallel Distributed Processing, as Artificial Intelligence was often called at the time. The school also offered courses in neurocomputation, which UC Berkley didn't at the time, otherwise the more prestigious school. During the 18 months I commuted back and forth, often in the middle of UCSD classes, from California to Lund, where I was obliged to teach medical students' basic neuroscience as part of my doctoral studies, two things happened.

First, I ran into Jens Schouenborg. His research showed that the nociceptive withdrawal reflex seemed to be imprinted by a learning mechanism at the spinal cord level, rather than by genetic programming, as was commonly assumed. We agreed that, it would be highly relevant to see if a mathematical neural network approach could be found, using realistic biological principles, that explained and simulated the learning of the withdrawal reflex. After publishing an abstract in 1996, this mathematical model, much later, and with strong contributions from others, became a Nature paper (Paper V).

Second, I came up with an invention, where the use of artificial neural networks would, in my own words back then, revolutionize the manual microscopy of human blood smears and potentially all microscopic work in Pathology. Clearly, a neural network, I believed, would be superior to humans for this reasonable well-defined mathematical transformation task of classifying stained human blood cells on a microscopic slide. The idea to the company Cellavision AB (Reg. no 556500-0998) was born in 1993 and the company slowly started to grow. Soon the company was growing quickly, and I also started another company, again based on artificial neural

network ideas, and I found myself to entangled to be able to finish my PhD studies. Ever since, though, I have insisted, often to the laughter of my friends and colleagues, that I would soon make time and conclude my doctoral studies. Twenty years later, I guess all of us were right.

Unfortunately, in 2003 my supervisor, Professor Wolfgang Grampp, passed away all too early. Instead, a fellow PhD student from the time of my doctoral studies, now a distinguished researcher with his own research group, Associate Professor Henrik Jörntell, has been kind enough to take on the role as my supervisor in completing this thesis.

Original papers

This thesis is based on the following papers, which will be referred to by their roman numerals.

I.   **Fåhraeus, C.**, Borglid, K. & Grampp, W. (1997). Properties of electrolyte-filled glass microelectrodes: an experimental study. *Journal of Neuroscience Methods. 78 (1-2): 15-28.*

II. **Fåhraeus, C.** & Grampp, W. (1997). Properties of electrolyte-filled glass microelectrodes: a model analysis. *Journal of Neuroscience Methods. 78 (1-2): 29-45.*

III. Theander, S., Edman, A., **Fåhraeus, C.,** Akoev, G. N. & Grampp, W. (1999). Cl⁻ transport in the lobster stretch receptor neurone. *Acta Physiologica Scandinavica. 167: 285-98.*

IV. **Fåhraeus, C.**, Theander, S., Edman, A., & Grampp, W. (2002). The K–Cl Cotransporter in the Lobster Stretch Receptor Neurone - A Kinetic Analysis. *Journal of Theoretical Biology. 217(3):287-309.*

In addition, the following paper will be presented in this thesis, and referred to, by the fifth roman numeral.

V.   Petersson, P., Waldenström, A., **Fåhraeus, C.** & Schouenborg, J. (2003). Spontaneous muscle twitches during sleep guide spinal self-organization. *Nature. 424 (6944), 72-75.*

Introduction

Nervous system and electricity

The discovery that nervous tissue has electrical properties was made already 1791 with Galvani's famous demonstration where a frog muscle would contract when the leg nerve was connected to a metal conductor. The first publication of a single neuron electrical recording was done much later by Edgar Adrian in his 1928 publication "The Basis of Sensation". In this, he describes the recordings of electrical discharges in single nerve fibers, using a Lippmann electrometer. He won the Nobel Prize in 1932 for his work that revealed these new properties for neurons. However, it was only in 1939 the first intracellular recording of an action potential could be made, this time using an intracellular glass microelectrode (Hodgkin & Huxley, 1939), on the giant axon of a squid, surprising everyone, including the authors, on the sheer magnitude of the action potential spike. They too won the prize, in 1963, some 30 years after Adrian.

The glass microelectrode truly revolutionized intracellular recordings and gave birth to an era of endless discoveries of the machinery and channels responsible for the electrical properties of neurons, and microelectrodes became a principle tool to investigate the mechanisms and functions of the nervous system as a whole. Over the years, in addition to understanding the generation of action potentials, ion channel dynamics and synaptic integration, single neuron recordings continued to provide insight on topographical mapping in the cortex. In short, the use of intracellular glass microelectrodes has contributed to much of what we today know about neurons, channels, carriers, action potentials and synaptic activities. Microelectrodes have, arguably, without competition been the most important tool in electrophysiological work on neurons until the development of the patch clamp with gigaohm seal properties (Hamill et. al., 1981).

Intracellular microelectrodes are still indispensable in intracellular work, not least for cells embedded in surrounding tissue. But like other measurement tools microelectrodes are cursed with some imperfections, namely: (a) microelectrodes do not form a gigaohm seal with the membrane after penetration, which causes an unspecific leakage into the cell through the membrane around the electrode. This in turn depolarizes the membrane and increases the conductance of the cell; (b) microelectrodes often have tip potentials and these can distort voltage recordings

(Adrian, 1956; Agin & Holtzman, 1966; Schanne et al., 1968); (c) the electrolyte from inside the microelectrode is leaking into the cytoplasm of the impaled cell and is changing the transmembrane ion balance of the cell (Fromm & Schultz, 1981); and (d) many glass microelectrodes show strong current rectification which limits their experimental usage domain (Gestrelius et al., 1981).

Over the years, several of the microelectrode artifacts have been studied and theories have been presented in trying to explain them. The tip potential for example, has been thought to depend on fixed negative charges in the glass wall of the microelectrode (Schanne et al., 1968), which are affecting the mobility of the electrolyte ions differentially, or alternatively, to a semipermeable glass wall (Okada & Inouye, 1976), acting as a selective ion exchanger. For the leakage of potassium ions (K^+) from KCl-filled microelectrodes into the cell cytoplasm, some estimates have been obtained experimentally by $^{42}K^+$ efflux studies (Fromm & Schultz, 1981) and also by intracellular ion accumulation measurements (Isenberg, 1979; Blatt & Slayman, 1983) as well as by theoretical predictions. The current rectification properties have been thought to depend on electro-osmotic fluid transports across the tip opening of the electrode (Rubio and Zubieta, 1961; Firth and DeFelice, 1971).

However, there is no experimental data on the relative abundance of chloride (Cl^-) and potassium ions (K^+) leakage from KCl filled glass microelectrodes into the neuron, during current injection or in resting conditions. The latter information would be critical in bringing clarity to the Cl^- transmembrane balance and homeostasis in a neuron using glass microelectrode techniques.

Modeling the intracellular glass microelectrode

Despite the fact that intracellular microelectrodes have been extensively used for more than half a century, there are hardly any comprehensive theoretical models available. In fact, we have not been able to find any theoretical framework or a mathematical model that describes the full set of the microelectrode's electrical and electrochemical behavior in the literature. A potential hindrance in constructing a microelectrode model could be the impression that the properties of microelectrodes are governed by multiple physical, chemical, electrical and electrochemical laws which could make a model exceedingly complex, hard to verify and without strong prediction power. Nevertheless, a high validity microelectrode model, could clarify the behaviors of microelectrodes over a broader set of condition than experiments can address and therefore serve as a background framework for all work involving intracellular microelectrodes. Also, a model could be used for constructing microelectrodes with properties tailored for specific research or experimental purposes. Finally, a microelectrode model would be instrumental in studies on Cl^- homeostasis in neurons using microelectrode techniques.

Chloride ions and the nervous system

Chloride ions are the most abundant physiological anion in animal cells. Yet, the importance of chloride ions in cell physiology has not been fully recognized until recently, in spite of the fact that the transmembrane Cl^- gradient is crucial for excitability and synaptic inhibition (Alvarez-Leefman, 1990), cell volume control (O'Neil, 1999), pH regulation (Aickin, 1994), secretion (Begenisich & Melvin, 1998), and more recently, plasticity and learning (Staley et al., 1995; Wang & Kriegstein, 2008).

In the mammalian central nervous system (CNS), the intracellular Cl^- concentration of a neuron determines the polarity and magnitude, and hence the strength of GABAergic neurotransmission, the dominating inhibitory system in the CNS, and is therefore of pivotal importance for the integrative functions of the CNS. In the peripheral nervous system, glycine mediated synaptic inhibition is the most abundant inhibitory system, and again the Cl^- gradient determines the polarity of the post synaptic potential and therefore its efficiency.

When $GABA_A$/glycine receptors are activated, chloride ions either leave or enter the cell through the respective ionophores, depending on the equilibrium potential for Cl^- relative to the membrane polarization. If chloride extrusion mechanisms are prevalent, thus keeping the Cl^- equilibrium potential below the membrane potential, chloride enters the cell on $GABA_A$ activation which leads to hyperpolarization, but if chloride transport into the cell dominates, $GABA_A$ activation leads to depolarization, instead of the typical inhibitory action. It is therefore not surprising that disruption of Cl^- homeostasis in neurons is associated with pathological conditions. From the literature epilepsy (Delpire, 2000; Okabe et al., 2002; Cohen et al., 2002; Woo et al., 2002), brain ischemia (Mu et al., 2017), and neuropathic pain (Coull et al., 2003) have all been implied in, or correlated with, transmembrane Cl^- transport aberrations. Most interestingly, intracellular Cl^- is also ascribed an important role in adult plasticity (Staley et al., 1995) and a pivotal role in neonatal plasticity and synaptogenesis (Leinekugel et al., 1997; Wang & Kriegstein, 2008).

Cl^- transporters

Intracellular Cl^- levels should be largely set by the balance between membrane potential, abundance of a Cl^- leak channel system, activation state of voltage or ligand gated Cl^- channels such as $GABA_A$, the presence of Cl^- transport systems such as the K-Cl cotransporters (KCCs) and Na-K-2Cl cotransporters (NKCCs), the Cl-HCO_3 antiports, and finally putative Cl^- pumps (Hara et al., 1993, Gerencser & Zelezna, 1993). In general, Cl^- linked H^+ antiports are believed to be responsible for pH adjustments rather than bulk Cl^- adjustments and should not have major impact

on the Cl homeostasis. In our preparation, the neurons are impaled with intracellular 3.0 M KCl filled glass microelectrodes, so the leakage of chloride ions from the microelectrodes will also play a major role in the cells Cl^- homeostasis and in setting the intracellular Cl^- concentration.

Despite the fundamental role Cl^- is playing in all animal nervous systems, few transmembrane analyses of the Cl^- homeostasis machinery exist in the literature. Specifically, investigating the K-Cl cotransporter and the Na-K-2Cl cotransporters role under varying conditions, would be important for a fuller understanding of the transmembrane Cl^- balance, since these cotransporters are believed to be the main mechanisms for determining the intracellular Cl^- concentration in neurons.

Quantifying the K-Cl cotransporter

K-Cl cotransporters (KCCs) exist in all tissues of mammals and are probably abundantly expressed throughout the animal kingdom. It is generally believed that the K-Cl cotransporter is the key protein for setting the Nernst potential for Cl^- below the resting membrane potential in the mammalian CNS, and in other nerve cells with an inhibitory $GABA_A$ innervation. An interesting observation is that a developmental delay in the expression of the K-Cl cotransporter and an increased expression of the Na-K-2Cl cotransporter is believed to be the dominating reasons behind the excitatory effect of GABAergic neurotransmission in the immature mammalian CNS (Payne et al., 2003), pointing to an instrumental role of this cotransporter in determining the chloride balance also in the developing brain, and thereby, possibly, in enabling the CNS to modify, discover and tune it's wiring (Wang & Kriegstein, 2008).

Despite its obvious importance no one has quantitatively characterized the K-Cl cotransporter in a neuron to our knowledge. Such a quantification, capable of dealing with biologically relevant variations in the concentrations of the substrates Cl^- and K^+, intracellularly and extracellularly, would be critical to fully understand and model a neuron with a functional $GABA_A$ inhibitory machinery.

To measure a zero current, such as the K-Cl cotransporter current, where K^+ and Cl^- fluxes are expected to be equal and thus producing no net current, poses a challenge. However, certain observations can bring some clarity. For instance, during voltage steady state, the sum of all membrane currents, irrespectively of ionic species, has to add up to zero, or the membrane potential would change. Further, during ionic steady state, the sum of all currents for each ionic species, must also add up to zero, or the intracellular concentration of that ion would change. Specifically, this must be true for K^+ and Cl^-, the substrates of the K-Cl cotransporter. The research group of the late professor Grampp has long been investigating the stretch receptor neuron and have a good quantitative understanding for the most relevant channels and

currents, under resting conditions and during impulse firing (Edman et al., 1983; 1986; 1987a; 1987b; Gestrelius & Grampp 1983; Theander et al., 1996; 1997). Using such knowledge, it should in theory be possible to calculate the K-Cl cotransporter's transport rate for Cl^-, as the negative sum of all the other Cl^- currents and, partly independently, for the K^+ transport rate, from the negative sum of all the other K^+ currents in the preparation (including intracellular microelectrode currents).

Mathematical simulation of Cl^- turnover in a full neuron model

The intracellular Cl^- concentration will not only vary with the expression degree of the K-Cl cotransporters (and Na-K-2Cl cotransporters), but also during dynamic events such as simultaneous application of excitatory and inhibitory stimuli, which is likely to occur frequently in our preparation and in the mammalian CNS, and changes in extracellular Cl^- or K^+ concentrations, likely to occur after intense firing or in hyperosmotic challenges. Also, cell variables such as the permeability of K^+ and Cl^- channels, transport capacity of the cotransporters and the activation state of K-Cl cotransporters (and Na-K-2Cl cotransporters) in the membrane, will also be important in determining the intracellular Cl^- concentration. In general, when there are a number of subsystems involved in a biological process, the various ways these can interact are often hard to intuitively predict. As has been noted above the intracellular Cl^- concentration is dependent on both the activity of the cell and the relative abundance and activation state of the membrane proteins shuffling Cl^- across the membrane, but also on the gradients of other ions that are part of the total cell's ion homeostasis.

As noted above, the intracellular Cl^- concentration is determining the effects of inhibitory drive thus setting the excitability in the nervous system, is critical for pH regulation and has been implicated to be instrumental in plasticity (Leinekugel et al., 1997; Wang & Kriegstein, 2008). Taking all this into account, it seems fruitful to construct a computational model of not only the K-Cl cotransporter but of the full neuron, to be able to assess the relative contribution of the various factors influencing the intracellular Cl^- concentration in resting and dynamic conditions. Such a model could shed light on questions for the functional role of the cotransporter that is hard to investigate with precision in real life.

Learning hypothesis in the CNS for reflexes

Learning

In the late 19th century, Cajal and Golgi presented beautiful and accurate images of a plethora of different neurons in the CNS, using the recently invented and further improved Golgi staining method. Based on these stained neurons, as viewed through the microscope, Cajal proposed the so-called "neuron doctrine", which said, contrary to common belief at the time, that neurons were discrete entities and separated from each other. He also proposed that communication between neurons took place through a specialized region in the synaptic tree, what we today call the synapse, and even proposed that strengthening connections between existing neurons could be the base for memory (Croonian Lecture, 1894). He received the Noble Prize for his neuron discoveries in 1906.

However, it was not until the 1940's when theoretical work by Hebb (1949) and later Rosenblatt (1958) showed the power of the idea of synaptic strength modifications as a basis for memory and information processing. Rosenblatt's machine, the Perception, propelled the first hype in AI, not to different from todays, with US government putting enormous funds into AI based research, to achieve machine translation from the Russian language to the English, as part of the cold war spending (Crevier, 1993). Hebb's original rule of learning, in the book "The Organization of behavior" (1949), was formulated "When an axon of cell A is near enough to excite a cell B and repeatedly or persistently takes part in firing it, some growth process or metabolic change takes place in one or both cells such that A's efficiency, as one of the cells firing B, is increased."

In 1966, Hebb's idea finally got strong experimental support, by work in the hippocampus by Terje Lømo (1966). In these experiments, it was shown, that if a certain group of neurons were stimulated intensively for a short period of time, the synaptic strengths between them and the postsynaptic firing neurons, were potentiated for considerable time. This was eventually named Long Term Potentiation (LTP), and the paper by Bliss and Lomo (1973) triggered a whole field of research. Later it has also been shown that channels such as the NMDA receptor are critical for memory formation and that plasticity can be severely impaired by blocking these pharmacologically. This strengthen the hypothesis that the learning rule postulated by Hebb seems to be of relevance in our studies. Interestingly, depolarizing post synaptic potentials from the $GABA_A$ receptor, implying high intracellular Cl^-, are believed to play a pivotal role in starting synaptic tuning, mediated by NMDA and AMPA receptors, in the immature CNS (Leinekugel et al., 1997; Wang & Kriegstein, 2008).

The withdrawal reflex

The spinal cord is the place were all sensory information first enter the CNS and were all motor commands leave the CNS. All tactile primary sensory neurons are synapsing before or in the spinal cord, and all motoneurons in direct contact with effector muscles, are located within the spinal cord. Therefore, studying the spinal cord have always been an important aspect of understanding also higher centers in the CNS, and in particular the various reflexes, where all processing typically takes place inside the spinal cord.

The nociceptive withdrawal reflex is a defense mechanism to protect the body from damage, where essentially the body moves away from noxious stimuli by activating an appropriate set of muscles, minimizing tissue damage. In the beginning of 20th century, this system was studied extensively by Sherrington and others. Based on these studies the nociceptive withdrawal reflex were described as "flexion reflexes" denoting the activation of flexor muscles while simultaneously inhibit extensor muscles upon noxious stimuli (Sherrington, 1906; Sherrington, 1910). For a long time, this concept has been prevailing despite the fact that also extensor muscles were shown to have receptive fields that activated reflex contraction (Hagbarth, 1952; Engberg, 1964).

The first conclusive publications for a different concept came in the early 1990's (Schouenborg & Kalliomäki, 1990). In these experiments a much more detailed topographic organization for the nociceptive withdrawal reflex was described. Further, it was shown that each muscle had its own receptive field and that the receptive field of each muscle basically was the withdrawal pattern caused by activation of the same muscle (Schouenborg and Kalliomäki, 1990; Schouenborg et al., 1992; Kalliomäki et al., 1992). Later, it was also shown that in the deep dorsal horn there are interneurons, connecting to motoneurons, that have identical receptive fields as single hindlimb muscles (Schouenborg et al. 1995).

Learning the withdrawal reflex

For a long time, spinal reflexes have been assumed to be hardwired and independent of experience (Brodal, 1992). This notion has several problems, such as the very large information storage requirement in the DNA for encoding an efficient withdrawal reflex. Also, since it involves a nonlinear sensorimotor transformation for each unique individual body constitution, there are challenges to keep the reflex adequate during growth. Finally, there seems to be an obvious risk for DNA mismatch when generating offspring, since the DNA coding for one's unique 3D shape may not follow the DNA coding for one's withdrawal reflex.

As of now, nobody knows how the accurate, and seemingly nonlinear, transformation from nociceptive stimuli to motor output is created. Yet, several lines

of evidence are suggesting that the connections of the polysynaptic withdrawal reflex are the result of a tuning algorithm rather than a result of genetic programming.

First, it is known that transplantation of Dorsal Root Ganglia's' to a novel neuroaxis position in the chick embryo creates new peripheral innervation patterns and new connection patterns in the spinal cord (Smith & Frank, 1987). Second, translocation of a muscle, thus changing the biomechanics of withdrawal, also changes the cutaneous field activating said muscle (Holmberg et al., 1997). Third, the close correlation between individual muscles biomechanical withdrawal fields and the receptive fields for the nociceptive withdrawal reflex of the same muscle, is tempting to see in the terms of an evolutionary opportunity. Why wouldn't evolution use a way to copy this map instead of hardwiring another one with obvious risks for mismatching?

It is therefore of utmost interest to investigate if a biologically plausible learning algorithm that solves this problem efficiently, fast and accurately could be found.

Many of the simulations and the mathematical model for the unsupervised learning theory, using spontaneous muscle twitches for the adjustment of the spinal withdrawal reflex, have been presented earlier in preliminary form (Fåhraeus et al., 1996).

Aims

The aims of this thesis were

1. To understand how intracellular microelectrodes are affecting neuronal ion homeostasis, excitability and physiology by characterizing experimentally and explaining theoretically (i) the classical microelectrode artifacts, such as rectification, and tip potential and (ii) the electrolyte leakage from the microelectrode tip into a model neuron, in particular quantifying the Cl^- leakage, during intracellular current injection and during passive electrodiffusion (Paper I and Paper II).

2. To examine and describe the Cl^- turnover in a neuron preparation, in particular how transmembrane chloride transporters affects the Cl^- equilibrium potential and the polarity of the inhibitory post synaptic potential of the neuron (Paper III), and to quantitively characterize and mathematically model a K-Cl cotransporter in order to analyze the role of the cotransporter in setting the inhibitory post synaptic driving force, in volume regulation and in combatting transient high extracellular potassium (Paper IV).

3. To investigate, by a mathematical model of the spinal withdrawal reflex system, if an unsupervised correlation-based learning mechanism, using fetal spontaneous muscle twitches, can explain the development of an adequate withdrawal reflex in mammals (Paper V).

Methods

Characterizing KCl leakage from intracellular microelectrodes (I, II)

Preparation of microelectrodes (I, II, III, IV)

In the standard case, single-barrelled microlectrodes were pulled from filamented borosilicate glass capillaries (Hilgenberg, D-34323 Malsfeld, Germany) with outer and inner diameters of 1.8 mm and 1.2 mm, and a filament diameter of 0.18 mm. After backfilling with 3.0 M KCl, the electrodes were bevelled according to Clementz & Grampp (1976) until their resistances assumed "typical" values, R_{typ}, around 10.5 MΩ in a grounded 0.1 M KCl immersing solution. R_{typ} was defined as the average ratio between transelectrode voltage transients and ± 2 nA transelectrode square current pulses, 0.15 ms after the onset of each current pulse at zero background current. For some experiments, single-barrelled electrodes were filled with 0.5 M KCl or 2.0 M KCitrate, but otherwise treated as the standard electrodes. In the case of the 0.5 M KCl-filled electrodes, this meant that the value of R_{typ} amounted to levels around 32.1 MΩ.

Equipment for measurements of the electrical and geometrical electrode properties (I)

For the measurement of electrical microelectrode properties, a standard electrometer unit (with an input time constant of 30 μs and a typical current leak of <5 pA) with a current generator for transelectrode current passage (0 - 500 nA through an output time constant of 10 μs) was used. Voltage and current signals were evaluated from oscilloscope screen photographs.

For the measurement of microelectrode tip potentials, V_t, electrodes had their distal tips, about 50 μm long, broken off in an electrically grounded 0.1 M KCl immersing solution, resembling intracellular in composition. The changes of the transelectrode voltage was, after reversing their signs, taken as tip potentials. For measurements of time-dependent transelectrode I-V curves, recordings were made of voltage responses from a 20 s long square current pulses of either polarity and with varying

amplitudes. The maximum time length of the current pulses was chosen to allow the current-voltage relationships to assume near-steady state values (Fig. 1A and 1B).
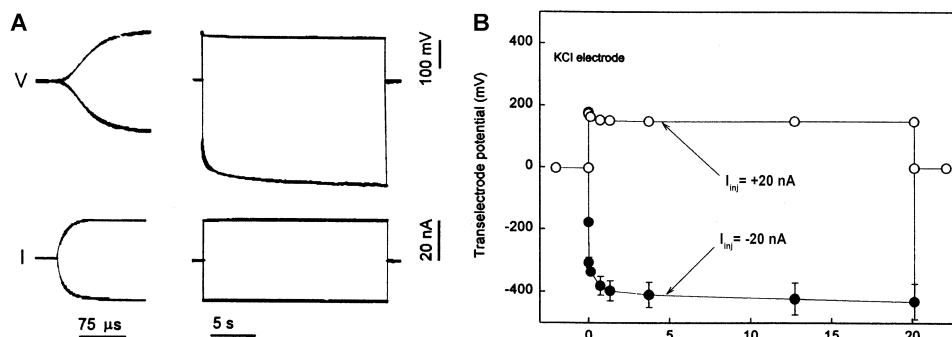

Figure 1. Electrical properties of 3.0 M KCl-filled microelectrodes immersed in 0.1 M KCl solution. **A**, Oscilloscope recordings of transelectrode voltage responses, *V*, to square current pulses, *I*, of ± 20 nA, in higher and lower time resolution. The initial relative slowness of the voltage response to the current pulse is due to the electrode capacitance. **B**, Transelectrode voltage responses from six different electrodes to ± 20 nA transelectrode square current pulses. The error bars in B, represent SE.

For the measurement of geometrical properties by scanning electron microscopy, electrodes were backfilled with filtered 3.0 M KCl solution and beveled as above. After measuring their resistances, the electrodes were thoroughly washed free from their KCl filling by filtered distilled water. Then, the electrodes were emptied and left to dry at room. After this, their tips were glued with epoxy resin onto metal discs, coated with 13 nm of gold and finally viewed and photographed in a scanning electron microscope (Philips SEM 515).

Production of radioactive tracer material and electrodes with radioactive filling (I)

For preparing solutions containing high concentrations of $^{42}K^+$ and/or $^{38}Cl^-$, 99.5% pure KCl, 99.8-100.2% pure $KHCO_3$, and 99% pure CholineCl salts (Sigma, St. Louis, MO. 63178 USA) were exposed to thermal neutrons for 24 h in a nuclear research reactor (Studsvik Nuclear AB, S-61182 Nyköping, Sweden). After this exposure, both ^{42}K and ^{38}Cl and, also, some other isotopes such as ^{32}P and ^{35}S, were detected in significant amounts.

Because of the short half-life of ^{38}Cl (37.2 min), and for safety reasons all experiments involving radiotracer measurements were done in laboratories close to with the reactor facilities. All times for tracer measurements will refer to zero time, T = 0 min, being the time of retrieving the radioisotopes from the reactor.

Electrodes were with a 3.0 M solution of radioactive KCl. After this, electrodes were prepared for beveling. It was found that the electrodes retained high resistances in

spite of beveling in the beginning, possibly for the reason that gas bubbles were formed in the electrode tips from water radiolysis in the presence of very high radiation intensities. However, after some 30 min this complication stopped and electrodes could be beveled as described above, resulting in a regular electrode production from T = 42 min.

Procedures for producing and measuring radiotracer fluxes from microelectrodes (I)

For spontaneous (purely diffusive) effluxes, electrodes were, after rinsing their tips in large amounts of 'cold' 0.1 M KCl solution, held motionless into a counting vial for 10 min about 7 mm deep in 7 ml of a 'cold' 0.1 M KCl solution. For current-driven effluxes, electrodes were, after rinsing their tips, connected to an electrometer amplifier/current generator probe and then held motionless into counting vials, immersed about 7 mm deep into 7 ml of an electrically grounded 'cold' 0.1 M KCl solution. Upon immersion of the electrode tips into the KCl solution, currents of about ± 10 nA, ± 20 nA, and ± 40 nA were passed through the electrodes for 140 or 240 s, using one counting vial for each of the total of 6 current passages.

Before measuring the radiotracer activities, 5 ml of scintillation fluid (Optiphase 'Hisafe' three, Wallac Sverige AB, S-19481, Upplands Väsby, Sweden) was added to the 7 ml of KCl solution in the counting vials, including the blank samples. After this, measurements of radiotracer activities were performed in a liquid scintillation counter (LAB Wallac 1219, Wallac Sverige AB, S-19481, Upplands Väsby, Sweden) recording all beta decay in 1024 energy windows. Counting times were optimized with respect to the ^{38}Cl decay pattern.

Evaluation of radiotracer measurements (I)

For radiometric measurements on samples, they show not only activities from ^{42}K and ^{38}Cl but, also, of other non-^{42}K/^{38}Cl isotopes. Therefore, we needed to isolate the various activities from each other. This isolation was done by means of the least square method, after determining the specific decay spectra for ^{42}K, ^{38}Cl, and the non-^{42}K/^{38}Cl isotopes. After this, the isolated activities were used to compute currents corresponding to the leakage of K^+ and Cl^- from the microelectrode tip.

For background corrections, background activities were determined in 4 blank samples (7 ml of 0.1 M KCl solution + 5 ml of scintillation fluid) for 10 min, at T = -1 h, T = 5 h, T = 73 h and T = 246 h. Since these activities proved to be the same at the 4 instants of time, an average background pattern was computed and, after adjustments for counting times, subtracted from all other tracer measurements.
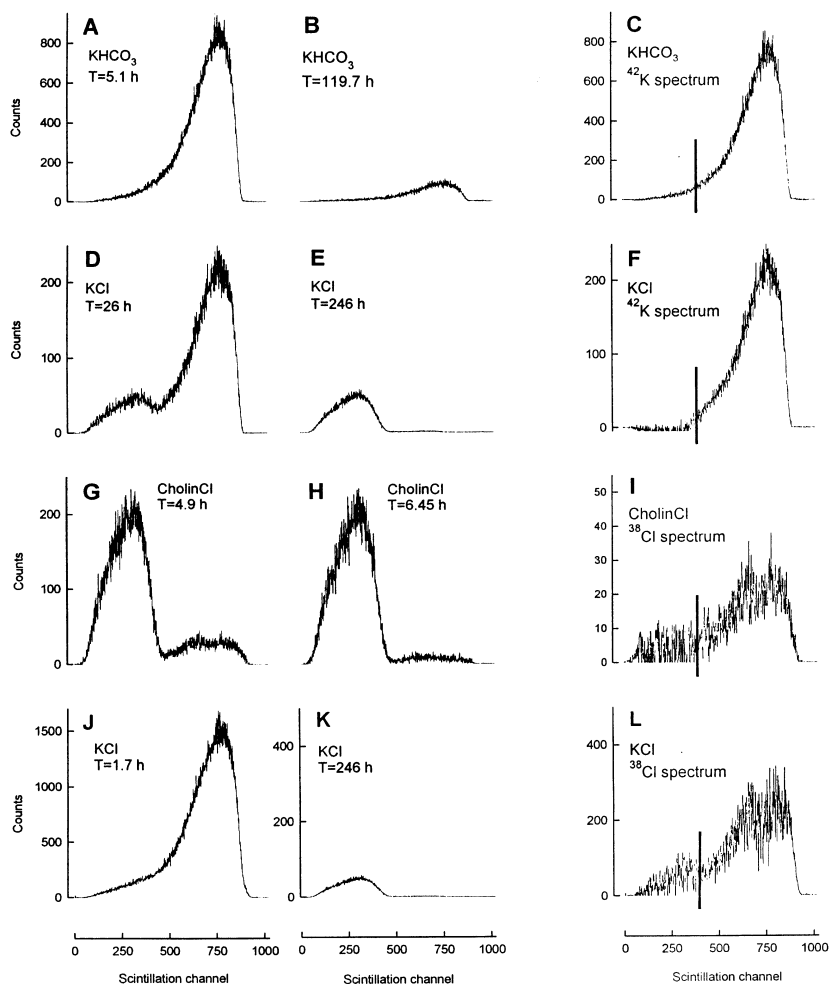
Figure 2. Deduction of specific decay spectra for ^{42}K and ^{38}Cl.
The individual panels in the left and middle columns show average decay spectra obtained on activated KCl, KHCO$_3$, and CholineCl, at times as indicated. The panels in the right column show the specific decay spectra obtained as follows: C=A - B (B representing conditions after the complete disappearance of ^{42}K), F=D - E (D representing conditions after the complete disappearance of ^{38}Cl and E representing conditions after the complete disappearance of ^{42}K), I=G - H (H representing conditions after the virtual disappearance of ^{38}Cl), and L=J - F* - K (F* representing the specific ^{42}K spectrum, F, adjusted to T-1.7 h and K representing conditions after the complete disappearance of ^{42}K). The vertical bars in the right column delimit the scintillation channels 1–380 whose signals were excluded from further data evaluation, since they were adding to noise more than to relevant information.

For the determination of specific decay spectra for ^{42}K and ^{38}Cl, activated KCl, KHCO$_3$, and CholineCl were diluted in 0.1 M 'cold' KCl solution to give practical decay intensities in four reference samples each. The activities in these samples were then measured shortly after preparation of the samples and, later, at times for the disappearance of ^{42}K and ^{38}Cl activity. The averaged results of such measurements are shown in Fig. 2 together with the specific decay spectra for ^{42}K and ^{38}Cl, calculated through subtraction of the composite spectra. The subtraction

26

method was considered appropriate on the ground that non-^{42}K/^{38}Cl radioisotopes, which could be expected to occur in the reference samples, did so either with concentrations too low or with half-life times too long to affect the estimates. Closely similar decay spectra were calculated for ^{42}K, independently of starting with KHCO$_3$ or starting with KCl. For ^{38}Cl the same is true independently off starting from CholineCl or KCl.

Decay spectra for non-^{42}K/^{38}Cl activities were determined using samples of activated KHCO$_3$, CholineCl, and KCl, after complete disappearance of ^{42}K and ^{38}Cl. The results of such measurements are displayed in Fig. 3. They show that the rest activities found in the KHCO$_3$ samples are undistinguishable from the background activity (Fig. 3E), and that the remaining activities found in the KCl and CholineCl samples are characterized by decay spectra that rise to significant levels and, also, are closely similar to each other (Fig. 3C and 3F). From the last it is concluded (a) that a non-^{42}K /^{38}Cl activity does exist and must be accounted for in any subsequent data analyses, and (b) that, with respect to what types and quantities of long-lived isotopes are created through activation of Cl-containing substances, the non-^{42}K/^{38}Cl activity can be attributed to ^{32}P in smaller, and ^{35}S in greater proportions.
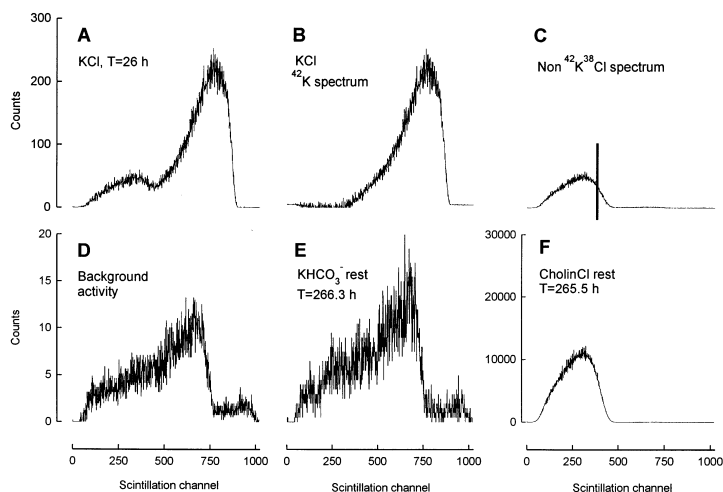
Figure 3. Deduction of a decay spectrum for non-^{42}K:^{38}Cl isotopes, and illustration of 'rest' and background decay spectra. The non-^{42}K:^{38}Cl spectrum was obtained as follows: C = A - B [A representing conditions after the complete disappearance of ^{38}Cl (same as D in Fig. 3) and B representing the specific ^{42}K spectrum (same as F in Fig. 3)]. The non-^{42}K:^{38}Cl spectrum is qualitatively indistinguishable from the CholineCl rest spectrum, F, obtained after the complete disappearance of ^{38}Cl and, because thereof, indicative of the samples containing no unaccountable contamination. E, HCO$_3$ rest spectrum after complete disappearance of ^{42}K. Statistically, this rest spectrum does not differ from the background decay spectrum (D) and, because hereof, indicative that no unaccountable contaminations are present in the material. The vertical bar in C delimits the scintillation channels 1–380 whose signals were excluded from further data evaluation, since they were adding to noise more than to relevant information.

Identification of ^{42}K, ^{38}Cl, and non-^{42}K/^{38}Cl activities from composite decay spectra by means of the least square method (I)

In view of the above it can be assumed that any composite decay spectrum, $\overline{DS}$, measured on a KCl-containing sample does represent a linear combination of the individual decay spectra for ^{42}K, ^{38}Cl, and the non-^{42}K/^{38}Cl isotopes. Formally, this can be expressed as

$$\overline{DS} = \alpha^{42_K}\overline{K} + \alpha^{38_{Cl}}\overline{Cl} + \alpha^N\overline{N} \tag{1a}$$

Where $\overline{K}$, $\overline{Cl}$, and $\overline{N}$ denote the decay spectra for ^{42}K, ^{38}Cl, and the non-^{42}K/^{38}Cl isotopes each normalized to unity and not including any signals from scintillation channels 1-380, since these appeared to contribute to noise more than to any significant information (cf. Figs. 3C and 2C), and the coefficients α^{*x} the number of decays for the various isotopes in a given sample at the time of scintillation analysis.

By constructing a matrix, Q, where $\overline{K}$, $\overline{Cl}$, and $\overline{N}$ are columns, Eq. (1a) can be rewritten as:

$$\overline{DS} = Q\overline{\alpha} \text{ with } \overline{\alpha} = (\alpha^{42_K}\alpha^{38_{Cl}}\alpha^N)^T \tag{1b}$$

Since Eq. (1b) consists of 644 linear equations with 3 unknowns, a solution exists only in the least square sense, meaning that the squared error of the solution $(\overline{DS} - Q\overline{\alpha})^2$, is reduced to a minimum. With such constraints, a solution can be found (Press et al., 1992) by multiplying Eq. (1b) with QT and inverting, such that

$$\overline{\alpha} = (Q^TQ)^{-1}\,Q^T\overline{DS} \tag{2}$$

An example of a solution derived in this way from an activity recording obtained at T = 144.5 min, representing a 10 min spontaneous KCl leakage from a single electrode, is displayed in Fig. 4. In A, it shows the specific decay spectra together with the underlying composite spectrum and in B, as a test of validity of the least square decomposing method, that the difference between the composite decay spectrum and the sum of all of its components is close to zero throughout the spectrum.
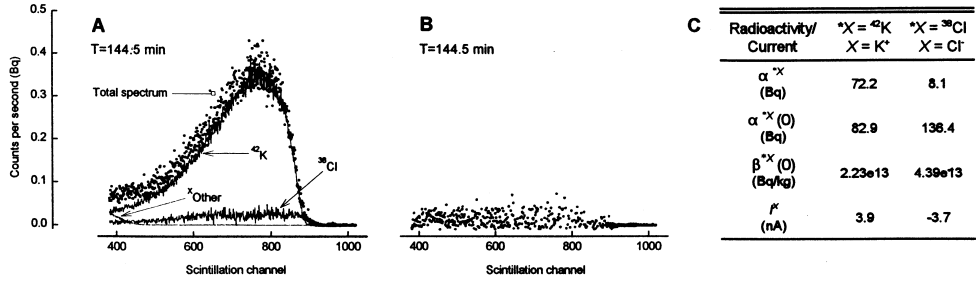
Figure 4. Decomposition. Decomposition of a radioisotope decay spectrum due to [42]K, [38]Cl and non-[42]K: [38]Cl isotopes leaving a microelectrode, at zero electrode injected current, and computation of K^{+} and Cl^{−} leakage currents corresponding to the isotope effluxes. **A,** Composite spectrum (dots) and pertaining [42]K, [38]Cl and non-[42]K: [38]Cl (Other) spectra (solid lines), as indicated. **B,** Validation of the decomposition (least square) method, by plotting the estimation error (difference between the composite spectrum and the sum of its three components) for each scintillation channel. **C,** Compilation of radiation data and pertaining ion currents deduced from the decay spectrum in A (see text).

Computation of K^{+} and Cl^{−} currents from [42]K^{+} and [38]Cl^{−} activities (I)

Following determination of the activities of the radiation source *X, α^{*X} at a time T, a value of $\alpha^{*X}(0)$, i. e. α^{*X} at T=0, can be obtained through the decay equation

$$\alpha^{*X}(0) = \alpha^{*X}/e^{-T \ln 2/T_{1/2}^{*X}} \tag{3}$$

in which $T_{1/2}^{*X}$ represents the half-life of *X.

Since specific activities (activities per mass of X) at zero time, $\beta^{*X}(0)$, can be deduced for *X = [42]K and *X = [38]Cl (see Fig. 4C) , computed values of $\alpha^{*X}(0)$, can be translated into mass of X and, further, into currents, I^X, carried by X (currents leaving the electrode are defined as positive currents), using the expression

$$I^X = \alpha^{*X}(0)z^X F/(\beta^{*X}(0)m^X \Delta t) \tag{4}$$

where F is the Faraday constant, z^X the valency, and m^X the molar mass of the current carrier X, and Δt the time during which the current flow is maintained.

An example of the results of doing so is given in Fig. 4C. It shows that the absolute values of the computed K^{+} and Cl^{−} currents are comparable to what had been observed in a previous study (Fromm and Schultz, 1981) and, also, that they are similar in size, as expected for an electroneutral electrolyte leakage from a microelectrode.

Simulation procedures (II)

Mathematical simulations of dynamic processes were achieved with the ADAMS integration method in the MATLAB/SIMULINK (The MathWorks, Inc., Natick, MA., USA).

Chloride homeostasis and dynamics – experiments and modeling (III, IV)

Preparation (III, IV)

All experiments in Paper III and IV were performed on slowly adapting stretch receptor neurons from the second and third abdominal segments of the European lobster (Homarus gammarus). For the measurements, stretch receptor organs were isolated and mounted in an experimental chamber, which was continuously perfused with solutions of desired composition at 18 degrees C.

In order to increase the electrophysiological homogeneity of the preparations, the axons of the receptor neurons were ligated with fine nylon threads at a distance of 600-800 μm from the cell body. This procedure had previously been found to have no negative effects on the cells' viability or firing behaviour and could be assumed to provide for a satisfactory (at least 90%) voltage control in voltage-clamp conditions, even in peripheral parts of the preparation (Gestrelius & Grampp, 1983). To eliminate accidental movements of the receptor muscles, these were crushed except for their central (intertendinous) region containing the dendrites of the receptor neuron.

During the experiments, the preparations were fully relaxed and no measurements begun until the receptor neurons had become stabilized completely with respect to membrane voltage and input resistance following microelectrode impalement. Typically, this period of stabilization took 30-60 min.

Solutions (III, IV)

The standard physiological saline had the following composition (in mM): NaCl 325, KCl 5, $CaCl_2$ 25, $MgCl_2$ 4, $MgSO_4$ 4, tris HCl 26, tris base 4, and glucose 5. The pH of the solution was adjusted to 7.3-7.4 by first bubbling it with 5% CO_2 in O_2 for 30-45 min and then titrating it with 0.5 M NaOH. The concentrations of CO_2

30

and HCO_3^- were thereby set to values not exceeding 0.15 mM and 1.5 mM, respectively. Solutions containing non-standard K^+ concentrations were prepared by varying the KCl content in the standard physiological saline without osmotic compensation. To all solutions, 480 nM tetrodotoxin (TTX), 10.0 mM tetraethylammonium (TEA), 0.5 mM 4-aminopyridine (4-AP) and 2.0 mM Cs^+ were added. This was done in order to eliminate action potential current and hyperpolarisation-activated Q-current components. Unless intracellular Cl^- measurements were performed by means of the GABA method (see below), 8.3 μM picrotoxin (PTX) was also added to the solutions in order to suppress any spontaneous post-synaptic inhibitory miniature potentials.

Measurements of electrical membrane properties (III, IV)

Membrane voltage and current measurements were performed with intrasomally placed double-barreled (one barrel for voltage recordings and the other for current recordings) microelectrodes. Both barrels were filled with 3 M KCl and had, after bevelling, typical resistances of 9-10 MΩ. Conventional electronic equipment was used for signal recording in both current- and voltage-clamp measurements.

Measurements of intracellular ion concentrations (III, IV)

Measurements of intracellular concentrations of H^+, Na^+ and K^+ were performed with intrasomally placed double-barreled ion-selective microelectrodes. One of the barrels, the reference barrel, was filled with a 0.5 M KCl in the case of Na^+, and H^+ measurements and 0.5 M NaCl in the case of K^+ measurements, and the other barrel with the adequate ionophore (all ionophores by Fluka Chemie AG, CH-9470 Buchs, Switzerland). The electrodes were calibrated using mimicking solutions and measurements were accepted only when identical pre- and post-experiment calibration curves were obtained.

Intracellular Cl^- concentrations were measured either directly with double-barreled ion-selective electrodes or indirectly via recordings of the membrane voltage in the presence of 1-2 mM γ-aminobutyric acid (GABA). The latter were conditions in which, during a 200-300-fold decrease in input resistance, the cell's membrane voltage became practically identical with its Cl^- equilibrium voltage and the intracellular Cl^- concentration therefore could be computed from the Nernst equation. When the doubled- barreled electrodes were used the reference barrel was filled with 0.25 M K_2SO_4 and the other barrel with a Cl^- -sensitive ionophore (by Fluka Chemie AG).

Numerical methods (IV)

Mathematical simulations of electrophysiological cell properties were performed by expanding a previously established FORTRAN-based model of the stretch receptor's transmembrane ion and current control (Söderlind, 1980; Gestrelius, 1983; Edman et al., 1986; 1987a; 1987b; Edman & Grampp, 1989; Edman et al. 1992). See also APPENDIX C of Paper IV.

Statistics (III)

Mean values are given with their standard errors (SEM). Levels of significance for differences between paired observations were computed using the two-tailed version of the Mann-Whitney U-test.

Learning movement patterns in the spinal cord (V)

Animals used

Wistar rats (P12–P17) of both sexes (n = 84 from 13 litters) were used.

Conditioning stimulation

During conditional stimulation, the spontaneous twitches were detected by a fast optical system (CMOS sensor camera; CCi4; C-Cam Technologies, acquisition rate, ~180 images s-1). Software written in LabVIEW 5.2 (National Instruments Corp.) was used to classify the movements. Twitches with a lateral deviation of the midsection of the tail more than 9.2 radians s-1 (~0.28 m s-1) after more than 300 ms of immobility triggered an air-puff directed to the side of the tail (Fig. 5A). The air-puff had a peak pressure of ~20 kPa and stimulation latency from twitch initiation of ~40 ms at normal tail position. The time-point and direction of stimulation were stored by the system. Conditioning stimulation was given for 2–3 days per animal. The uncorrelated stimulation was given at random to either side of the tail. Trained animals did not differ from untrained animals of the same litter with regard to body weight or overall behavior.
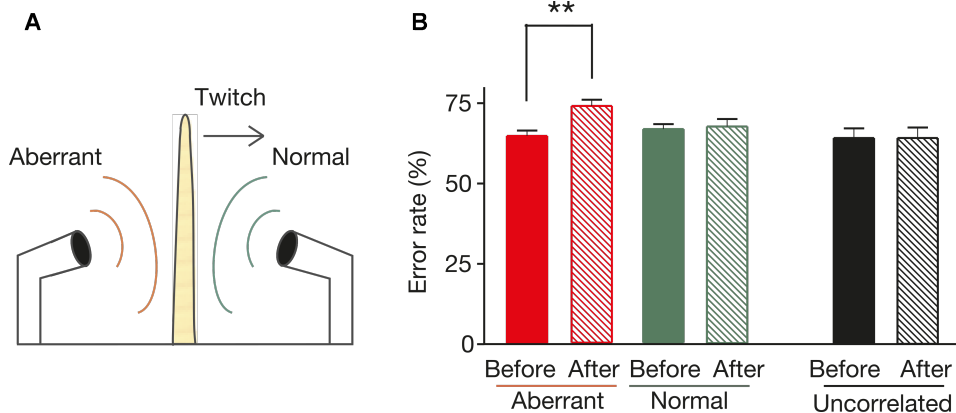
Figure 5. Behavioural experiments.
A, Schematic training set-up showing the aberrant and normal training protocols. **B,** NWR error rate before and after aberrant, normal or uncorrelated stimulation; results are means + s.e.m. The NWR error rate was significantly increased (**P < 0.01) in rats given aberrant tactile feedback (49 training sessions); normal air-puff stimulation (54 training sessions) had no significant effect (Kruskal–Wallis and Dunnett's test). Controls with random air-puff stimulation (23 training sessions) or no stimulation (23 training sessions; not shown) did not affect NWR adaptation (P = 0.65 and P = 0.37, respectively; Wilcoxon signed-rank test).

Nociceptive withdrawal testing

Every test included 10 stimulations (25-ms CO_2-laser pulses, 5 W, beam width 3 mm) to each side of the distal tail; the persons performing the analyses were blinded to the type of conditioning stimulation used. Response latencies were monitored in all NWR testing experiments; owing to the increase in animal size, the mean latencies increased from 156 to 179 ms during the P12–P17 period (mean of the s.e.m. = 2.1 ms), indicating C-fibre evoked reflexes. Only tail-tip movements of more than 0.02 radians ~1 mm) were considered.

Computer simulations

The simulations were implemented in MATLAB. Experimental data, needed for the simulations, consisted of six movement patterns produced by five different muscles (peroneus longus (PL), peroneus brevis (PB), tibialis anterior (TA), gastrocnemius (G) and two subunits of the extensor digitorum longus with tendon insertions on digits 2 and 3 (EDL23) and digits 4 and 5 (EDL45). The data were represented in 28 x 61 matrices (597 of these matrix elements represented sites of the plantar skin and were used in the simulation, representing >1.5 pixels mm-2 in an adult). The data were sampled by optical three-dimensional movement analysis yielding the velocity component perpendicular to the skin surface for 40–50 individual skin sites. Matrix values for intermediate sites were interpolated by spatial low-pass filtering (Schouenborg & Weng, 1994). These patterns were assumed to describe the pressure changes on the plantar skin in the hindlimb in standing position and consequently the pattern of afferent input (pressure changes) from mechanoreceptors responding to skin pressure on muscle contraction. Quantified and normalized nociceptive withdrawal receptive fields (intramuscular electromyographic recordings) of the muscles were obtained from previous studies (Schouenborg & Weng 1994). For each learning epoch, muscles were activated at random with a specified probability. On co-activation of muscles, the withdrawal movement was approximated as the sum of the normalized withdrawal patterns of the individual activated muscles. The cutaneous feedback, which was represented on the same coordinates as the withdrawal efficiency, is conveyed by parallel afferents reaching 597 first-order interneurons in substantia gelatinosa (SG_j). These, in turn, act on six reflex-encoding deep dorsal-horn neurons (RE^k). Hence, 597 connection weights (w_j^k) between substantia gelatinosa neurons and reflex encoders for each of the six modules were updated in each learning epoch. A total of 10,000 epochs was estimated to correspond roughly to the observed number of tail twitches during the adaptation period (Waldenström et al., 2002). Oja's rule, $\Delta w_j^k = \eta RE^k(SG_j - RE^k w_j^k)$, where η is the learning rate, was used for synaptic weight adjustments (w_j^k normalizes to $w_j^k \in [0, 1]$) (Oja 1982; Turrigiano et al.1998; Fregnac et al. 1998; Katz & Shatz, 1996). In then motor-directed somatosensory imprinting (MDSI) scheme, a learning epoch is initiated by a burst in the reflex-

encoding neuron ($RE^k \neq 0$). Parameter values in the simulation shown in Fig. 6A and C had the following settings: a learning rate η of 0.008, a twitch probability per module for each epoch of 0.045 (resulting in $\sim\frac{1}{4}$ of the epochs containing twitch activity in at least one of the six modules and $\sim$11% coactivity), sensory noise $\in$ $[-0.5, 0.5]$ ($\pm 50\%$ of maximum tactile input), and initial synaptic weights w_j^k were randomly drawn from a uniform distribution $U[-0.8, 0.8]$. The model was effective within a relatively wide range of parameter values. Mean adult correlations of at least 0.8 were reached for $\eta \in [0.0053, 0.043]$, twitching probability $\in$ $[0.03, 0.24]$ (yielding 7.5–55% co-activity), sensory noise $\in [-3.9, \ 3.9]$ and initial synaptic weights drawn from $U[-3.2, 3.2]$ if these parameters were altered one at a time. Using only the contaminating movement patterns on co-activation, 0.11 is the maximum twitch probability that still satisfies a mean adult correlation of more than 0.80.
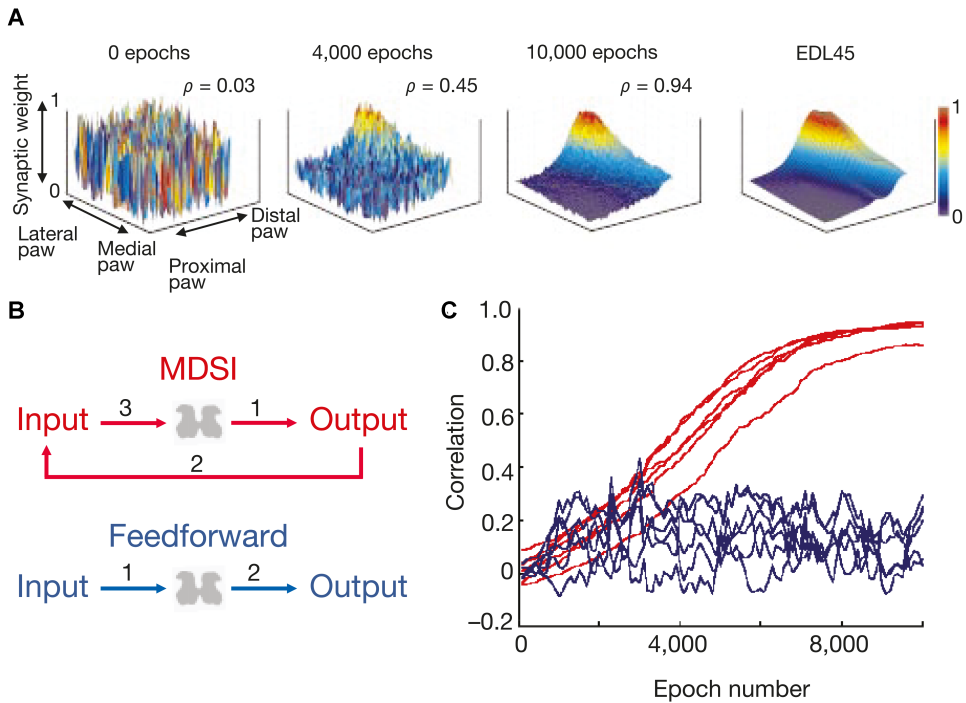
Figure 6. Simulated developmental adaptation of receptive fields for five muscles.
A, Simulated synaptic weight distributions of a receptive field (EDL45) at different timepoints during reflex adaptation. **B,** The two simulated learning principles: motor directed somatosensory imprinting (MDSI) and feedforward learning. The sequence of events is numbered. **C,** Simulated reflex adaptation curves. Correlations between synaptic weight maps and movement patterns (597 skin sites) at different time points for the respective muscles with the use of Oja's learning rule for six networks during MDSI (red) or feedforward learning (blue). Simulated (MDSI) and experimental adult correlations, respectively: r_{EDL23} = 0.94 and 0.91, r_{EDL45} = 0.93 and 0.95, r_G = 0.85 and 0.95, r_{PB} = 0.94 and 0.88, r_{PL} = 0.93 and 0.91, r_{TA} = 0.93 and 0.90.

In the simulation of unsupervised feedforward learning, learning occurs when the postsynaptic activity in the reflex-encoding neurons exceeds ~15% of the maximum response. Increasing the activation probability did not improve adult correlations. When activated, weight adjustments were performed exactly as in MDSI learning.

Results

Experimental characterization of intracellular microelectrodes (I)

For the characterization of glass microelectrodes it is realized that, ultimately, the properties of a glass microelectrode must depend on the geometrical dimensions, the glass composition, the electrolyte filling solution and the immersion solution.

From our scanning electron microscope measurements, it is was found that our typical glass microelectrode, used in most intracellular recordings of our preparation (Paper III & IV), has a tip opening diameter of 0.25 μm and an initial taper (diameter growth rate at the tip) of 0,0215 $\mu m/\mu m$ and an instantaneous resistance of 9 MΩ in artificial sea water solution when filled with 3.0 M KCl. By measuring several electrodes beveled to different tip diameters, and with different tip taper, it was found that the resistance is inversely proportional both to the tip diameter, and to the taper at the distal part of the microelectrode, this observation will later be used as a test of a theoretical model and simulation of the glass microelectrode (Paper II).

For an assessment of chloride equilibrium in the stretch receptor neuron (Paper III and IV), the relative contributions of K^+ and Cl^- in spontaneous leakage from the microelectrode (zero current) and during various levels of current injections, is needed. From nuclear plant experiments, we could deduce the unique decay spectrum of ^{38}Cl and ^{42}K and thereby, by using the least mean square method, decompose the total decay spectrum into the ^{38}Cl and ^{42}K components. After translating the activities of the two isotopes (^{38}Cl /^{42}K) to time zero, the corresponding K^+ and Cl^- currents could be calculated. Interestingly, it is found (Fig. 7B), that a significant part of all currents, negative or positive, are carried by K^+, and that Cl^- contributes only with around 20% for negative and positive currents. In the Discussion of Paper II we will take another look at this numbers, but the concept that K^+ carried currents dominate, remains. Another important observation (Fig. 7A) is that during zero current injection (spontaneous leakage), a background leakage of 3.8 nA for K^+ and -3.7 nA for Cl^- is observed. This non-trivial flux of K^+ and Cl^- is thus loading any impaled neuron throughout the entire experimental procedure when using standard 3.0 M KCl single-barreled glass microelectrodes, as a

minimum estimation. Any current injection schemes will likely increase these fluxes significantly.
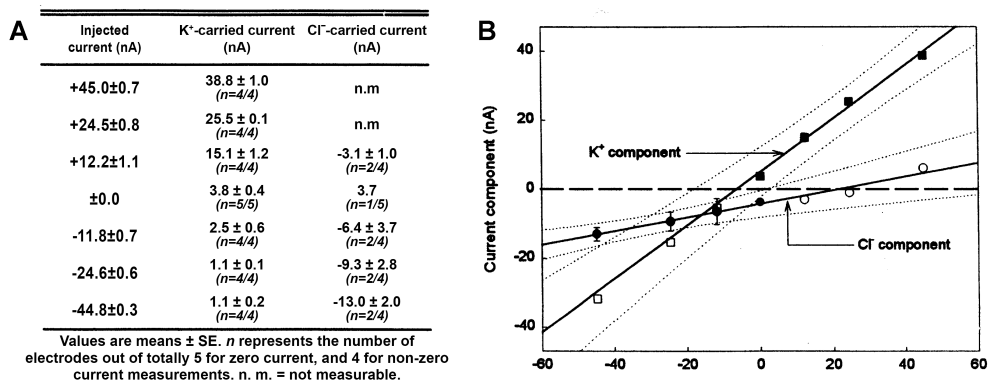

A

Injected current (nA)	K$^+$-carried current (nA)	Cl$^-$-carried current (nA)
+45.0±0.7	38.8 ± 1.0 (n=4/4)	n.m
+24.5±0.8	25.5 ± 0.1 (n=4/4)	n.m
+12.2±1.1	15.1 ± 1.2 (n=4/4)	-3.1 ± 1.0 (n=2/4)
±0.0	3.8 ± 0.4 (n=5/5)	3.7 (n=1/5)
-11.8±0.7	2.5 ± 0.6 (n=4/4)	-6.4 ± 3.7 (n=2/4)
-24.6±0.6	1.1 ± 0.1 (n=4/4)	-9.3 ± 2.8 (n=2/4)
-44.8±0.3	1.1 ± 0.2 (n=4/4)	-13.0 ± 2.0 (n=2/4)

Values are means ± SE. *n* represents the number of electrodes out of totally 5 for zero current, and 4 for non-zero current measurements. n. m. = not measurable.

Figure 7. Relationships between transelectrode driving currents and its K$^+$ and Cl$^-$ components. **A,** Compilation of K$^+$ and Cl$^-$ -carried current components deduced from the leakage of ^{42}K$^+$ and ^{38}Cl$^-$ from the electrode at various driving currents. **B,** Relationships between driving currents and their K$^+$ and Cl$^-$ components. The solid symbols correspond to measured current component values as shown in A, and the open symbols are current components deduced by subtracting the measured current component (solid symbol) from the total injected current. The solid and the dotted lines represent linear regressions, and their 95% prediction intervals, from the measured current component values. The slopes of the regression lines and the corresponding correlation coefficients are, respectively, 0.77 and 0.99 for the K$^+$ component, and 0.20 and 1.00 for the Cl$^-$ component.

Finally, the electrical electrode properties and its dynamics were studied. Importantly, the tip potential was found to be almost identical for electrodes filled with 3.0 M KCl and 0.5 M KCl, despite a difference of six times in electrolyte concentration. Further, the tip potential's absolute value was found to be inversely proportional to the tip opening, or in other words, proportional to the resistance of the electrode.

For the dynamical electrical properties of a 3.0 M KCl filled microelectrode a marked rectification takes place within fractions of a second (Fig. 8A). By studying this phenomenon in different filling solution (Fig. 8B) but with a constant immersion solution (0.1 M KCl), it is clear that with a filling solution of 0.5 M KCl, much of the rectification disappears. Corroboratively, when the immersion solution, with fixed filling solution, is varied from the standard value of 0.1 M KCl, to 0.8 M KCl and finally to 3.0 M KCl, the rectification entirely disappears (Fig. 8C). This strongly indicates that the rectification is a function of the difference in the filling and immersion solution, with strong rectification when the solutions differ the most and no rectification when the solutions are then same.
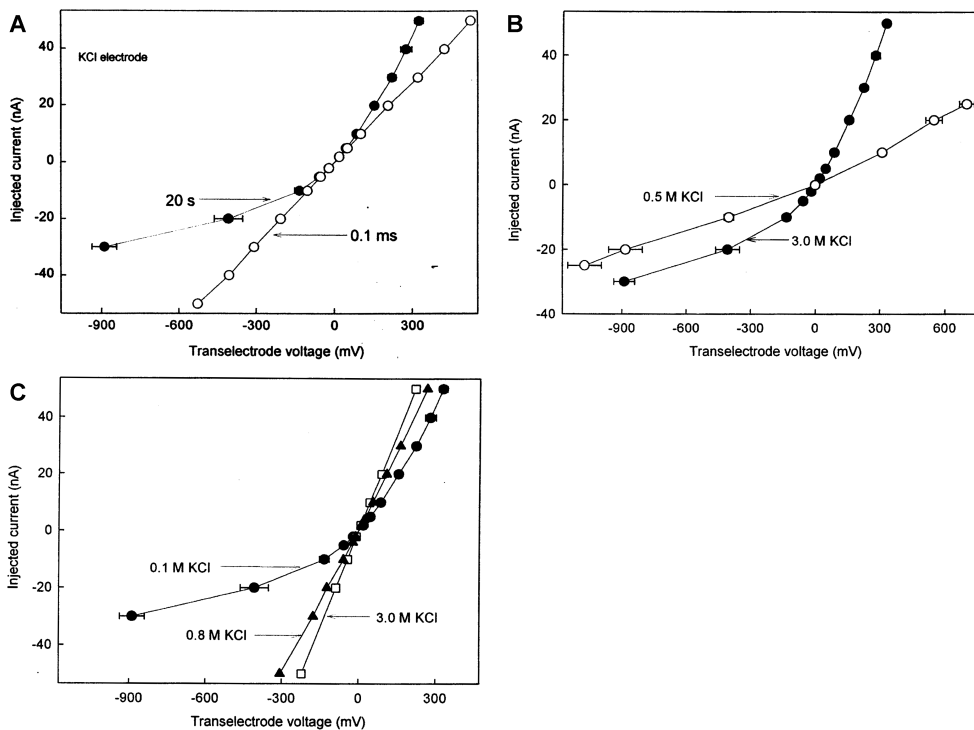
Figure 8. Transelectrode current–voltage (I-V) relationships.
A, I-V curve from six different electrodes representing conditions at 0.1 ms and 20 s after onset of the transelectrode current flow. **B**, I-V curve after 20 s of transelectrode current flow in four electrodes filled with 3.0 M KCl, and four electrodes filled with 0.5 M KCl solution. All eight electrodes were connected to grounded 0.1 M KCl solution. **C**, I-V curve after 20 s of transelectrode current flow in six different electrodes connected to grounded immersing solutions containing 0.1 M, 0.8 M, or 3.0 M KCl, as indicated. The error bars in A, B, and C (partly covered by the symbols) represent SE.

Theory and simulations of intracellular glass microelectrodes (II)

In Paper I we were able to establish a thorough understanding of the behavior of intracellular microelectrodes in terms of K^+ and Cl^- passage, tip potentials and rectification properties from various experiments.

For modelling the intracellular glass microelectrode (II), we assumed that both electrodiffusive and electroosmotic forces are at work. In brief, electrodiffusive forces are expected for charged particles diffusing in an electric field, as will certainly be the case during current injection through the microelectrode, but also during stationary conditions due to the finding of a microelectrode tip potential (Paper I). Further, fixed charges are often found in glass-water interfaces (Agin, 1969; Krischer, 1969a, 1969b; Lavallée and Szabo, 1969). This could explain the tip potential as a differential permeability of Cl^- and K^+ at the orifice of the

electrode, since a difference in permeability would naturally occur if fixed surface charges existed on the glass inner wall. Finally, the fixed charges could also be he bases for electroosmotic forces, indeed implied by the phenomenon of strong current rectification described in Paper I.

For the electrodiffusive particle flow, the Nernst-Planck flux equation can, in our case, be formulated as an ion current I_{ed}^X

$$I_{ed}^X = AFD^X z^X \kappa^X \left(\frac{d[X]}{dx} + [X] \frac{d \ln \gamma^X}{dx} + \frac{z^X F}{RT} [X] \frac{dV}{dx} \right) \qquad (5)$$

with κ denoting the relative molar conductivity for ion X and γ the activity of X at concentration $[X]$. κ and γ are thus modifying the effective concentrations for the ions in the equation.

The electroosmotic flow v, which will come out as the solution of the Navier-Stokes equations for flow velocity, if one combines them with the Poisson-Boltzmann equation for the interface charges between glass and electrolyte. By assuming that the thickness of the electrical double layer, the Debye length δ, is smaller than 1/20th of the radius of the electrode it can be shown (Rice and Whitehead, 1965) that the electroosmotic volume flow v is

$$v = A \left(\frac{\varepsilon \zeta}{4 \pi \eta} \frac{dV}{dx} \right) \qquad (6)$$

Where ζ is the potential at the plane of shear between the fluid's more structured and more diffuse part of the electrical double layer.

The associated ion current from the electroosmotic flow will be

$$I_{eo}^X = AF z^X [X] \left(\frac{\varepsilon \zeta}{4 \pi \eta} \frac{dV}{dx} \right) \qquad (7)$$

Finally, the total ion currents, $I^X = I_{ed}^X + I_{eo}^X$, are coupled to the concentration $[X]$ at all times by the continuity equation

$$\frac{d[X]}{dt} = \frac{I^X}{z^X F vol} \qquad (8)$$

Where $\frac{d[X]}{dt}$ is the time derivative of the concentration for ion X, into and out from the volume *vol*.

For the equations to make practical sense they were placed into the geometry of our intracellular microelectrodes and populated with the ions and concentrations from our experiments. Before doing the actual simulation, a mesh (or grid) was created as an approximation for the physical continuum assumed in the equations (Fig. 9). The mesh size was determined by comparing simulations with different mesh size until no or insignificant differences in output were observed by comparing the simulations.
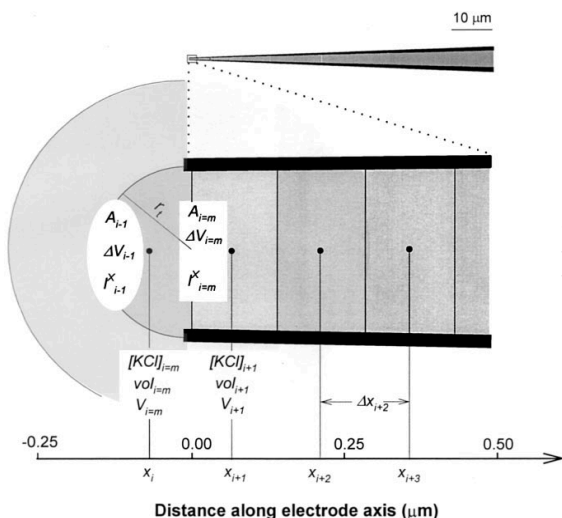

Figure 9. Mesh model of the electrode. Illustration of the model electrode tip (in low magnification, upper drawing) and its opening together with immersing fluid segments (in high magnification, lower drawing). Shown are, in particular, (i) the principle of dividing the fluid space from the immersing solution into the electrode filling solution and (ii) the relation between fluid segments, segment interfaces, and segmentally defined parameters.

All variables, except two, were taken without adjustment from either the geometry of the electrode or from standard textbook values. The two exceptions, both associated with the negative surface charges on the glass inner wall, are the zeta potential ζ, and the electrical double-layer thickness, the Debye length δ. These two values were chosen based on their fit to experimental data. Importantly, it should be noted that the data set for the parameter fitting consisted of only the steady state IV curve for the standard 3 M KCl electrode immersed in 0.1 M KCl solution (Fig. 7B rectification), no other data was used. The Debye length was adjusted to the tip potential on this IV curve, i.e. when the current injection was zero, and the zeta potential adjusted to give the right rectification on the curve. It should further be noted, that the values obtained for the zeta potential ζ and the Debye lengths δ, are in full agreement with expected ranges for glass-solution interfaces. In simulations with other filling solutions is was assumed that the Debye lengths was inversely proportional to the electrodes filling solutions concentration of ions, in accordance with the literature (Agin, 1969; Lakshminarayana, 1984).

In order to test the model's predictive power, and hence the validity of the model, simulations were setup according to the experimental protocol of Paper I, to evaluate the fit. In Fig. 10 the results of such simulations are presented, with experimental data appearing as circles, filled or not, in the diagrams. The 20 s. I-V curve of Fig. 10A, is the only curve that has been used for model adjustments, the others are used for model verification. It is clear that all curves in In Fig. 10 are reproduced with great fidelity, including the instantaneous I-V curve (the electrode resistance) (Fig. 10A), the stationary I-V curves for different electrode tip openings (Fig. 10B), and the I-V curves in different filling and immersion solutions (Fig. 10C and D).
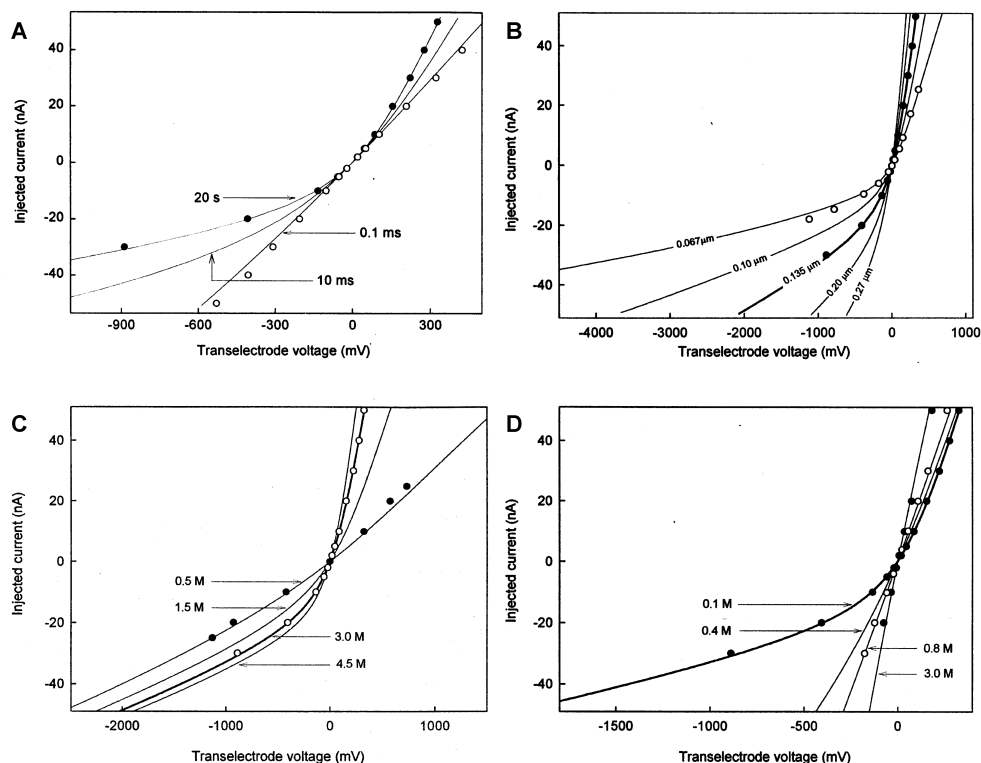
Figure 10. Transelectrode current-voltage (I-V) curves.
A, I-V curves at various times from onset of current flow. **B**, Steady state I-V curves at various tip radius openings. **C**, Steady state I-V curves at various [KCl] in the electrode filling solution. **D**. Steady state I-V curves at various [KCl] in the immersing solution.

For final tests of the model's validity we looked at the classical microelectrode artifact, the tip potential, and the typical resistance, where we had experimental data available. The model is again reproducing data very nicely, with verifications of the

electrode's tip opening radius' inverse relationship to the tip potential (Fig. 11B) and to the typical resistance (Fig. 11A). Interestingly, the model is also reproducing the non-trivial experimental finding, that lowering the electrolyte filling concentration does not change the tip potential in any significant way (Fig. 11D).
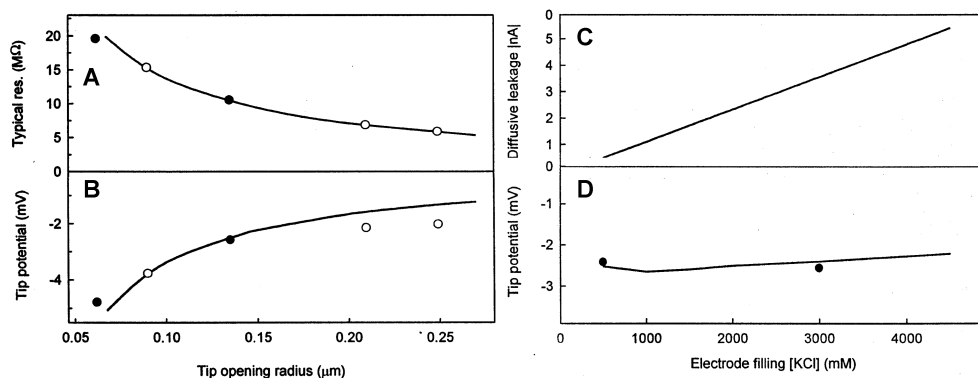

Figure 11. Relationships between tip radius and electrolyte filling solution and various electrode properties.
A and **B,** Steady state relationships between tip radius and typical electrode resistance and tip potential. **C** and **D,** Steady state relationship between [KCl] in the electrode filling solution and diffusive electrolyte leakage and tip potential. The circles in (A), (B) and (D) represent experimental data described in Paper I; the closed circles are implying direct r_t measurements, while the open circles are implying model-based r_t estimates from R_{typ} measurements.

Based on the tests of the electrode model's fidelity we find it likely that the model has high validity and we will therefore adopt it as a microelectrode theory and use it as a tool to generate simulations where experiments are scarce or hard to perform, but also for exploring microelectrode properties when they are given non-standard parameter values. These simulations will be addressed in the Discussion part of Paper II.

Intracellular chloride homeostasis and dynamics (III)

For an analysis on how the intracellular Cl^- concentration is maintained and dynamically altered in the stretch receptor neuron of the European lobster, it was decided to investigate the cation coupled Cl^- cotransporters, K-Cl and the Na-K-2Cl, in more detail. They are supposedly the main mechanisms for setting intracellular Cl^- in neurons, and no information regarding these exists in our cell. Also, it was decided to address the existence of putative Cl^- pumps in our neuron, since these could, in theory, have a major impact on the Cl^- homeostasis.

From the literature it is speculated that an ethacrynic acid sensitive (Hara et al. 1993) or orthovanadate sensitive (Gerencser & Zelezna, 1993) Cl^- pump exists in certain preparations. In order to test this in our preparation, we first treated our cells with 10-100 μM sodium orthovanadate, after blocking the Na-K pump by 5 mM ouabain, the latter was blocked to exclude any effect of the sodium orthovanadate on the Na-K pump. No changes in input resistance or membrane potential was observed. When trying instead with 300 μM ethacrynic acid, a minor increase in membrane potential (2.1$\pm$0.5%), and a statistically significant (17.3$\pm$4.0%), reversible, increase in intracellular chloride concentration was observed. However, if the increased intracellular Cl^- concentration is caused by shutting down a primary Cl^- pump, the pump must be outwardly directed. Then, blocking the putative Cl^- pump, must give a hyperpolarization, but no such thing is observed. Further, ethacrynic acid is a known loop diuretic, so the increased Cl^- concentration could also be assumed to come from blocking an electroneutral co-transporter. This would be in better harmony with the lack of hyperpolarization. Since the literature evidence is scarce for the existence of primary Cl^- pumps in neurons, and our experiments do not imply them, we concluded that they do not exist in our cell.

The next transporter to assess was the Na-K-2Cl cotransporter, known to be inhibited by 10 μM bumetanide in a variety of preparations such as smooth muscle cells (Smith & Smith, 1987), glial cells (Chassande et al., 1988) and the squid giant axon (Altamirano et al., 1995). However, no changes were detected in membrane potential, input resistance, nor in intracellular Na^+ or Cl^- concentrations after 10-30 minutes of exposure. It was concluded that the Na-K-2Cl cotransporter, if existing, does not play a significant role, under our experimental protocol in the preparation, and it will not be considered in our experiments. Nevertheless, we will elaborate more on this cotransporter in the Discussion section of Paper III and Paper IV.

Finally, testing for the existence of a K-Cl cotransporter, furosemide and the stilbene derivatives SITS and DIDS, all established blockers of the K-Cl cotransporter, were supplied in various concentrations. To rule out HCO_3^- coupled Cl^- transport, the experiments were performed in zero carbonate solution to start with. For all three drugs, there were dose dependent, reversible, Cl^- increases upon application. No consistent changes were recorded in membrane potential or input resistance of the cell. The latter was monitored by the effect of transient current pulses on the membrane potential. These observations are important since they strongly speak in favor of an electroneutral mechanism being responsible for the dose dependent, reversible, intracellular Cl^- accumulation. Further, choosing DIDS, showing the most powerful inhibition (lowest IC50) of this Cl^- extrusion system, tentatively the K-Cl cotransporter, experiments were performed in standard carbonate solutions (0.15 mM CO_2 and 1.5 mM HCO_3^-). From these experiments it is clear that there were no major deviations in the absolute values, nor any significant changes in the

overall dynamics, as compared to zero carbonate solution. Any Cl^- coupled HCO_3^- transport is therefore absent or negligible under our experimental circumstances.

In trials with KCitrate filled instead of KCl filled microelectrodes, also reversible intracellular accumulations of Cl^- occurred after application of DIDS, but as expected, these were much smaller in amplitude without the leakage of Cl^- from the KCl filled intracellular microelectrodes.

As a pivotal test of the existence of a K-Cl cotransporter the intracellular concentrations of Na^+, K^+, H^+ and Cl^- were monitored before, during and after applications of DIDS. From these tests it became clear that no changes in intracellular Na^+ or H^+ took place but that statistically equimolar changes in intercellular K^+ were observed in parallel to the changes in intracellular Cl^- (i.e. no statistically significant increase difference between Cl^- and K^+ were observed).

Lastly, from the literature it is known that 1 mM NEM (n-ethylmaleimide) can activate the K-Cl cotransporter, for instance in the mammalian erythrocyte (Lauf et al., 1992). After exposing the cells to NEM, the chloride concentration was significantly lower 5 minutes later, compared to control experiments (P<0.02). Since also the Na-K pump is known to be affected by NEM, the experiments were repeated after pretreatment with ouabain, the Na-K pump blocker. A decrease in intracellular Cl^- were observed under these conditions as well.

With these final pieces of evidence, it was concluded that the K-Cl cotransporter is existing and functionally significant in our neuron.

In order to study some potential functions of the K-Cl cotransporter, cells were exposed to high levels of extracellular K^+ in combination with an equimolar raise in extracellular Cl^-. In the absence of any blockers, there was an immediate change in the membrane potential due to the drastically changed equilibrium potential for K^+, the ion with the largest conductivity in resting conditions (first arrow in Fig. 12A). After this, the continued depolarization developed more slowly. Upon returning to standard physiological saline (SPS), the reverse happens, with an immediate polarization and then a continued, slower, return down to the original membrane polarization (second arrow in Fig. 12A). The shifts in intracellular K^+ (and Cl^-) as measured by K^+ selective microelectrodes placed in the cell soma (or Cl^- by GABA method), had no immediate phase, but a traditional accumulation curve in a finite volume during high K^+, and a traditional decay curve, returning to SPS. Repeating the experiments, but with DIDS blocking the co-transporter, two things were substantially different with respect to the membrane potential. First, the immediate phase of the voltage shifts, depolarization upon application of high external K^+, was significantly higher, almost reaching the final depolarization directly (third arrow in Fig. 12A). Second, the immediate phase of the polarization, upon returning to nominate K^+, was significantly stronger, almost directly returning to the resting

membrane potential in SPS (fourth arrow in Fig. 12A). With respect to the shifts in intracellular K^+ during DIDS exposure, the accumulation phase was more than 50% slower ($P<0.05$) and the unloading phase was very slow, even showing signs of not returning to baseline at all (Fig. 12A).
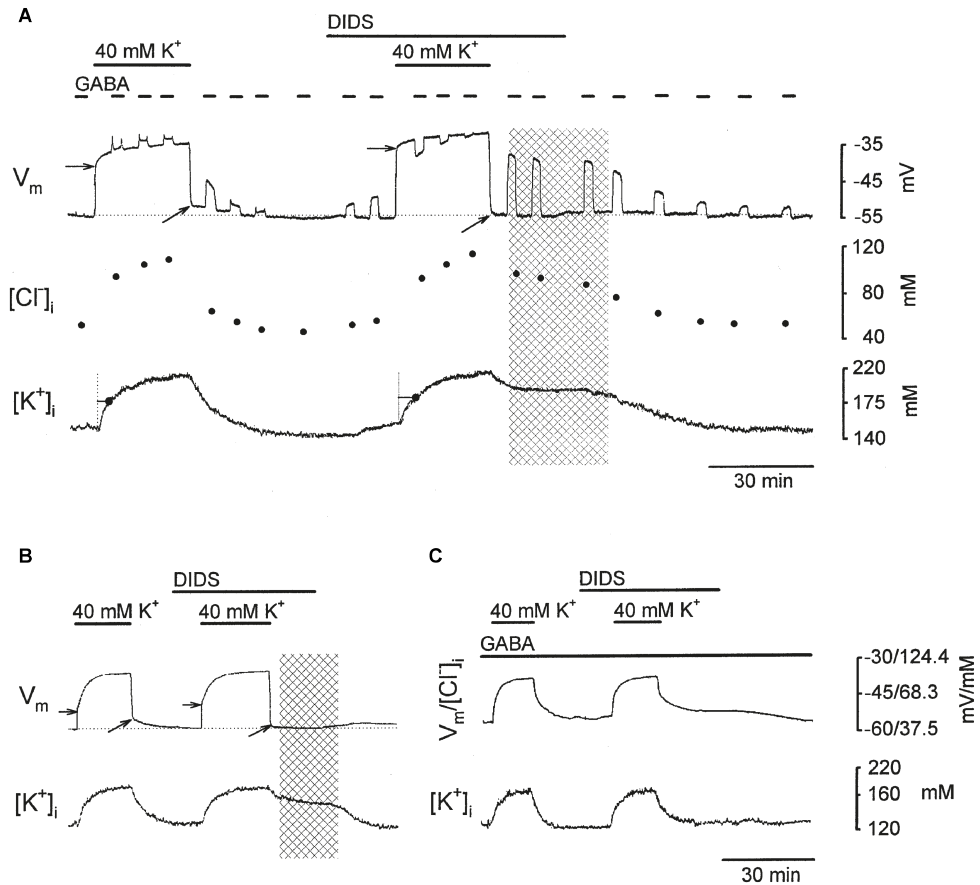

Figure 12. Effects on membrane polarization, V_m, and intracellular $[K^+]$ / $[Cl^-]$ after shifts in extracellular $[K^+]$ / $[Cl^-]$.
Effects of shifting the extracellular K^+/Cl^- concentration between 5/413 and 40/448 mM on V_m and intracellular $[K^+]$ and $[Cl^-]$ with or without DIDS. **A,** Simultaneous recordings of V_m, and intracellular $[K^+]$, by means of a K^+-sensitive electrode in the intermittent presence of 1 mM GABA (setting the membrane voltage to the Cl^- equilibrium potential from which the intracellular $[Cl^-]$ was computed) before, during, and after application of 0.2 mM DIDS. **B,** Simultaneous recordings of V_m and intracellular $[K^+]$ by means of a K^+-sensitive electrode before, during, and after application of 0.2 mM DIDS. **C,** Simultaneous recordings of V_m and intracellular $[K^+]$ on the same preparation as in B in the permanent perfusion of 1 mM GABA, before, during, and after application of 0.2 mM DIDS. In A and B the cross-hatched parts; cells are losing intracellular K^+ and Cl^- much more slowly in the presence of DIDS than without. In A the small horizontal lines with a right-hand dot, starting when changing intracellular $[K^+]$, mark the time for half-maximum intracellular K^+ accumulation.

To explain the difference in the dynamics of intracellular K^+ and Cl^- accumulation with or without DIDS, the following can be concluded. To change the intracellular K^+ concentration, two things are necessary, a sufficient transmembrane pathway for K^+ ions (assumed to exist through leak channels) and a sufficient transmembrane pathway for anions (or for a cation leaving the cell), since macroscopic electroneutrality must hold at all times. In DIDS, blocking the K-Cl cotransporter, it is logical to assume that a significant part of the transmembrane Cl^- transport becomes unavailable. Corroborating that a K-Cl cotransporter block is the explanation for the difference in dynamics, it is found that in continuous GABA perfusion, thereby opening up a large Cl^- conductance, the difference in KCl accumulation dynamics between DIDS and absence of DIDS, becomes negligible (Fig. 12C).

In contrast, the difference in instant membrane depolarization when exposed to DIDS and in the absence of DIDS, both in high extracellular K^+, cannot be explained by different dynamics for K^+ in the cell soma, the time constant for somatic accumulation of K^+ is to slow (Fig. 12A). However, two other possibilities exist. As noted above, the intracellular accumulation of K^+ (and Cl^-) in high extracellular K^+ is twice as fast with a functional K-Cl cotransporter, compared to a blocked one. This implies that there is a considerably flux of KCl into the cell, starting immediately upon perfusion of high extracellular K^+. The flux can affect the concentration of K^+ on both sides of the cell membrane. If intracellular diffusion of K^+ is to slow, an accumulation of K^+ immediately inside the membrane will take place, if extracellular diffusion is to slow, a depletion, immediately outside the membrane will take place. Either of these two possibilities will have an effect on the equilibrium potential of K^+ in the direction of less depolarization upon perfusion with high K^+, thus potentially explaining the membrane potential differences. Interestingly, direct evidence for an intracellular concentration gradient of 15 mM or more, from the immediate inside of the membrane to the bulk of the cell, has been reported for Na^+ and Cl^- (Fåhraeus & Grampp, 1993). Upon unloading, returning to SPS, the reverse would happen, with a relative (to the soma) depletion of K^+ and Cl^- on the immediate inside of the membrane. Evidence for a pericellular accumulation of K^+ has also been reported by Frankenhaeuser and Hodgkin (1956), but if this applies to our preparation during perfusion of high K^+ is not known.

In order to characterize the transport capacity of the K-Cl cotransporter in normal extracellular K^+ and Cl^-, cells in ionic homeostasis were exposed to DIDS in low carbonate solutions, both after impalement with KCitrate microelectrodes or after impalement with 3.0 M KCl microelectrodes. The increase in intracellular chloride, following application of DIDS, was assumed to be linear in short spans of time t at the beginning of the Cl^- accumulation. Then, the corresponding cotransporter Cl^- current I_{Cl}, could be calculated using the equation

$$I_{Cl} = Fvol \frac{\Delta[Cl^-]_{i,DIDS}}{t} \tag{9}$$

From Eq. 9, we calculate a value for ICl of 0.39 nA, when using KCitrate microelectrodes. In contrast, using 3.0 M KCl filled microelectrodes, the value is more than 10 times larger, 5.23 nA. It is interesting to note that, from Paper II, the calculated leakage from a double-barreled 3.0 M KCl filled microelectrode of the dimensions used in this experiment is 5.5 nA. This seems to anchor 5.23 nA, for the cotransporter current, as clearly having the right approximate size during impalement with double-barreled 3.0 M KCl filled electrodes.

Another useful data point can be deduced form Eq. 9. In the presence of DIDS, I_{Cl} must be the negative sum of by other Cl^- currents in the cell. These can be assumed to be genuine Cl^- channels, the impalement artifact Cl^- current and Cl^- leakage from the microelectrode. In the KCitrate electrode case, since the Cl^- leakage from the microelectrode must be zero, then, the sum of I_{Cl} must equal the sum of genuine Cl^- channel currents and the Cl^- artifact current. Further, assuming that the Goldman current equation can be used for both these currents, a total permeability P_{Cl} for Cl^- can be calculated. This value was found to be $2.2 \times 10^{-16} m^3 (s\ cell)^{-1}$, not to different from a previous study, using different methodology (Theander et al., 1996) of $1 \times 10^{-16} m^3 (s\ cell)^{-1}$ for the total Cl^- permeability when GABA channels are blocked by picrotoxin.

Modeling Cl^- dynamics in a neuron with a K-Cl co-transporter (IV)

To model the full receptor neuron with a particular focus on intracellular Cl^- dynamics, Cl^- homeostasis and cell volume control, it was decided to start with deducing a mathematical model for the K-Cl cotransporters, identified in paper III as the main mechanism for Cl^- extrusion in our cell.

In order to quantitatively assess the K-Cl cotransporter, it was fruitful to use the knowledge of our preparation in some detail, where we assume to have knowledge of (a) all the major Na^+, K^+ and Cl^- channels, (b) the Na-K pump, (c) the impalement artifact leakage and (d) the K^+ and Cl^- microelectrode leakage during current injection (zero or not).

In addition, for a mathematical deduction, we also need to make three biophysical assumptions.

First, the sum of all currents, in membrane polarization steady state, carried by Na^+, Cl^- and K^+, has to add up to zero. This assumption implies that the other ion currents are insignificant under the experimental protocol, which should be true given the low concentration of the non Na^+, Cl^- and K^+ membrane permeable ions and the low known permeabilities for the same. This assumption can be written

$$I_m = I_{Na} + I_K + I_{Cl} + I_{E,inj} = 0 \qquad (10)$$

The second assumption, valid for ion concentration steady state, is that for all currents carried by Na^+, Cl^- and K^+, the current sum for each ionic species must also be zero. This can be written

$$I_{P,Na} + I_{Imp,Na} = 0 \qquad (11a)$$

$$I_{P,K} + I_{Imp,K} + I_{L,K} + I_{El,K} + I_{C,K} = 0 \qquad (11b)$$

$$I_{Imp,Cl} + I_{S,Cl} + I_{E,Cl} + I_{C,Cl} = 0 \qquad (11c)$$

The third assumption is that the quantitative expressions, which are published for all the currents involved except the cotransporter I_C (Edman et al., 1983; 1986; 1987a; 1987b; Gestrelius & Grampp 1983; Theander et al., 1996; 1997), are sufficiently accurate to be used as tools in the deduction of I_C.

In principle we thus have two ways to quantify the K-Cl cotransporter

$$I_{C,K} = -(I_{P,K} + I_{Imp,K} + I_{L,K} + I_{El,K}) \qquad (11b')$$

$$I_{C,Cl} = -(I_{Imp,Cl} + I_{S,Cl} + I_{E,Cl}) \qquad (11c')$$

Where $I_{C,Cl} = -I_{C,K}$, assuming the cotransporter is electroneutral.

For the impalement artifact current $I_{Imp,Cl}$ and the GABA$_A$ operated synaptic current $I_{S,Cl}$, it was shown by Theander et al (1996) that they could be approximately

described by the Goldman constant field equation. For $I_{Imp,Cl}$ the expression becomes

$$I_{Imp,Cl} = P_{Imp,Cl}V_m \frac{F^2}{RT} \frac{[Cl]_o - [Cl]_i \exp{(-V_m\frac{F}{RT})}}{1 - \exp{(-V_m\frac{F}{RT})}} \tag{12}$$

In that study, the permeability for the impalement leakage $P_{Imp,Cl}$, was estimated to $5 \times 10^{-17} m^3 (s\ cell)^{-1}$, which is the value used in this study for all impalement permeabilities as well as for the synaptic leak permeability $P_{S,Cl}$. Corroborating the approximate size of this value, in Paper III we found the sum of $P_{Imp,Cl}$ and $P_{S,Cl}$ to be $2.2 \times 10^{-17} m^3 (s\ cell)^{-1}$, by an independent methodology.

The Cl⁻ carried microelectrode current is known from Paper II and can under stationary conditions be well approximated by a third-degree polynomial, as has been done in this publication for ease of calculation (Paper IV, APPENDIX B). With that, all the currents needed for the Cl⁻ component of the cotransporter are known, we now only need data points to populate Eq. 11c' over a relevant stretch of Cl⁻ and K⁺ concentrations, intracellularly and extracellularly. However, in order to give more robustness to the conclusions it was decided to make a partly independent calculation for the K⁺ portion of the K-Cl cotransporter.

Thus, turning to Eq. 11b', it is true that all currents are known from previous investigations, but since this investigation will deal with higher extracellular K⁺ concentrations than the existing experimental basis when calculating $I_{L,K}$ in Theander et al 1996, it was decided to expand the dataset and recalculate the previous parameter values for the K⁺ leak channel. The new values turned out to differ mainly with respect to the extracellular K⁺ modulating factor compared to previous publication (Theander et al., 1996).

The data points needed in Eqs. 11b' and 11c' (and also for a recalculation of $I_{L,K}$), were achieved by exposing cells in voltage clamp to sets of different extracellular K⁺ and Cl⁻ concentrations. In a 3.0 M KCl microelectrode impaled cell, the normal resting potential is around -65 mV, and this membrane polarization was chosen as the holding potential in all extracellular solutions. For each pair of extracellular K⁺ and Cl⁻ concentration, once a steady state was achieved with regard to current injection and intracellular ion concentrations, voltage steps were applied away from the -65 mV holding potential, and the corresponding current was recorded. Each such voltage step lasted 3 s. During each voltage step, the intracellular concentrations of K⁺ and Cl⁻ were assumed to remain unchanged. In this manner, for each pair of extracellular K⁺ and Cl⁻ concentration (and reciprocal intracellular concentrations) an I-V curve was constructed (Fig. 13). At each point on this I-V

curve it is true that $I_{E,inj}$ is equal to the negative sum of all other currents so by inserting Eqs. 11a-c into Eq. 10 and reshuffling, we get

$$I_{L,K} = -(I_{P,K} + I_{P,Na} + I_{Imp,Na} + I_{Imp,K} + I_{Imp,Cl} + I_{S,Cl} + I_{E,inj}) \qquad (13)$$

where the expressions and variables on the right-hand side are now known entities, including the measured entity, the injection current, $I_{E,inj}$. From this equation it is evident that any errors in the calculation of $I_{Imp,Cl}$ and $I_{S,Cl}$ will also affect $I_{L,K}$ but this error must be rather small. Thus, with all quantities on the right-hand side known we can now solve Eq. 11b' for $I_{C,K}$.

As a final note on the methodology it should be observed that intracellular Na^+ and H^+ did not change significantly during the experiments, which is important, since pH changes may alter the strength of the pump, in a way we have not compensated for in the calculation of the cotransporter current.

Once we have the data points for $I_{C,K}$ and $I_{C,Cl}$, which turned out almost identical, we need to decide on a mathematical format for the cotransporter. The simplest realistic model seemed to be the Hill equation for enzymatic binding. It was further reasonably assumed that the transport process was symmetric and that only the gradient of the product $[K][Cl]$ determines the direction for transport.

With these assumptions the expression becomes

$$I_{C,K} = I_{C,max} \left(\frac{n_c [S]_i^{n_c}}{[S]_i^{n_c} + K_{S,C}} - \frac{n_c [S]_o^{n_c}}{[S]_o^{n_c} + K_{S,C}} \right) \qquad (14)$$

with $[S]$ denoting the product $[K][Cl]$. Eq. 14 was found to give excellent reproduction of the derived experimental data, with the parameters fitted to the following values $I_{C,max} = 76.8 \times 10^{-9} A \ cell^{-1}$, $K_{S,C} = 4.75 \times 10^8 (mol \ m^{-3})^2$, and $n_c = 1.9$.

By inserting the expression for the cotransporter into a dynamic full-scale model of stretch receptor neuron (for details see Paper IV, Appendix C), comprising all the currents mentioned above but also the voltage gated channels for Na^+ and K^+ as well as a Q-current and an A-current, it was possible to test the effects of the cotransporter in whole cell simulations. By first testing the model to reproduce the data that is the base of the quantitative deduction, i. e. instantaneous membrane I-V curve in voltage clamp at different settings of extracellular KCl, it is evident that also the full receptor model is reproducing the data well (Fig. 13A). In addition, the

stationary intracellular KCl concentrations, are also faithfully predicted by the model, when starting with fixed extracellular KCl concentrations (Fig. 13B).
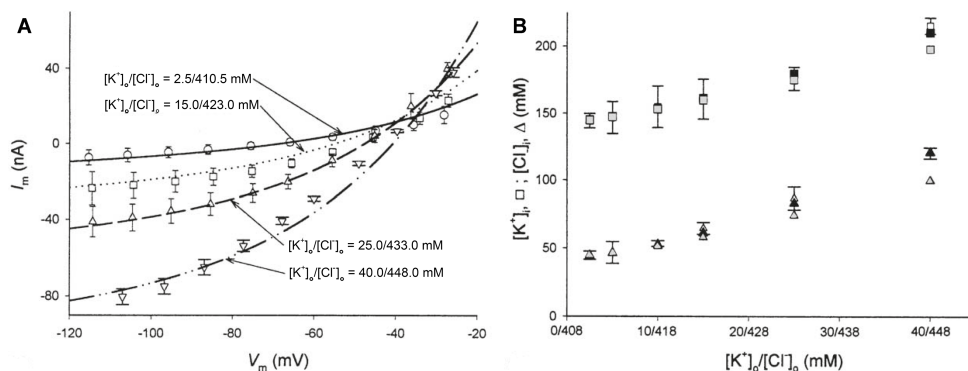

Figure 13. Full-scale receptor model predictions compared to empirical data.
A, ''Instantaneous'' voltage-clamp relationships between membrane voltage, V_m; and the total membrane current, I_m; around a steady-state holding voltage at -65 mV at various extracellular K^+/Cl^- concentrations. The open symbols and bars represent empirical data. The smooth curves are predictions by the receptor model at different extracellular K^+/Cl^- concentrations. **B,** Relationships between fixed extracellular K^+/Cl^- concentrations, and steady-state intracellular K^+/Cl^- concentrations. The open symbols (means ± SEM); correspond to experimental estimates, while the filled symbols represent model-predicted values from voltage-clamp at - 65mV (black symbols), and to current-clamp at zero-current injection (grey symbols).

Further, in conditions that played little part in the quantitative deduction, the model is reproducing experimental data from Paper III correctly, for instance in various blocking experiments of the K-Cl cotransporter. In these experiments, the predicted shift in intracellular Cl^- could be satisfactorily generated, sometimes better with a first order process for DIDS's blocking action, a refinement of the model that does make pharmacological sense.

Finally, the model could satisfactorily reproduce resting membrane potential, and resting intracellular Cl^- concentration, in cells impaled with either KCl-filled or KCitrate filled microelectrodes. The model, additionally, predicted shift in intracellular Cl^-, following a 300 s. blockade of the K-Cl cotransporter, that were close to the observed values in Paper III, for both electrode types.

Based on the tests performed we believe that the mathematical description of the cotransporter has validity and further that a dynamic model of the neuron, including the cotransporter, also behaves well. We therefore adopt the cotransporter and the neuron model as a hypothesis of this neuron's ion homeostasis and as a tool for further simulations. In such simulations we can deeper address some functions and implications of the cotransporter on, for instance, the excitability and ion homeostasis of the neuron.

Motor-initiated principle of learning the withdrawal reflex (V)

To investigate if a biologically realistic learning model could be found that explains and simulates the tuning of the withdrawal reflex, a mathematical model was constructed with components that agree with current neurophysiological knowledge.

Previously, the computational complexity to perform a non-linear composite multi joint sensorimotor transformation, such as the nociceptive withdrawal reflex has led researchers to propose multilayer network architectures (Pouget & Snyder, 2000). Multilayer networks, have indeed also been the focus of most theoretical and practical work in the broader subject of AI, ever since the limitations of the perceptron architecture became evident in the late 60's.

Further, up until recently, reflexes were believed to be hard-wired and independent of experience (Brodal, 1992).

However, a significant body of neurophysiological data is challenging these notions

I.   The spinal withdrawal reflex has a muscle-centric organization, or modular, where the withdrawal field of a muscle is the mirror image of the muscle's withdrawal efficiency from a surface (Schouenborg & Weng, 1994). Withdrawal patterns involving several muscles can be approximated as the linear sum of these muscles.

II.   Changing the innervation of the receptive field of a muscle (Holmberg & Schouenborg, 1996b) cause no aberrant withdrawal reflex, implicating that postnatal adjustments must take place.

III. Moving a tendon by postnatal surgery, which causes a new movement pattern for a muscle, still gives an adequate withdrawal reflex in the adult animal, that is adopted top the new movement pattern (Holmberg et al., 1997), again indicating adjustments.

Other observations that inspired us to propose a self-organizing model and algorithm for learning the nociceptive withdrawal reflex are

A.   During the period of development of nociceptive withdrawal reflexes, P1-P25 for rats (Holmberg & Schouenborg, 1996a), the most common movement patterns are muscle twitches, occurring in single relaxed muscles during sleep.

B.   Tactile input is necessary for normal development of nociceptive withdrawal reflexes, but nociceptive input is not (Waldenström et al., 2001).

C. The existence of interneurons, or premotorneurons, with identical withdrawal receptive fields as the muscle to which they had strong Connections (Schouenborg et al., 1995).
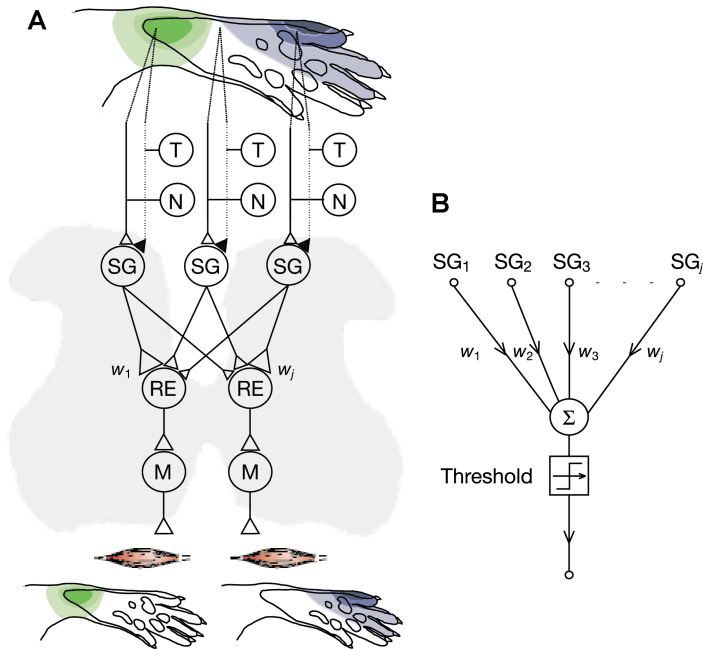

Figure 14. Proposed organization of a reflex module.
A, First, primary afferents feed into the reflex circuit monosynaptically or oligosynaptically (continuous or dotted lines); second, tactile (T) and nociceptive (N) inputs converge in substantia gelatinosa (SG) before reaching the reflex-encoding neurons (REs) located in the deep dorsal horn; third, SG to RE connections are specifically weighted (w_j = synaptic weights); fourth, REs have strong connections to motor neurons activating the muscle(s). The receptive and withdrawal fields of the gastrocnemius (green) and peroneus longus (blue) muscles, respectively, are shown. Filled boutons, inhibitory synapses; open boutons, excitatory synapses. **B**, A Rosenblatt perceptron for comparison.

Based on this, we propose a model architecture (Fig. 14A) for the nociceptive withdrawal reflex consisting of tactile input and nociceptive input, that together converge on interneurons in substantia gelatinosa (SG) in the superficial dorsal horn. These SG interneurons broadcast their signal to all the premotoneurons under study, called the reflex encoders (RE), situated deep in the dorsal horn. The reflex encoders connect to one motoneuron each, which in turn contract one effector muscle each. The architecture has an analogue in Rosenblatt's perceptron (Fig. 14B), where in this case the SG cells, together receiving a high number of tactile

and nociceptive input, converge on six reflex encoders, thus resembling six perceptrons, one for each effector muscle.

Further, we propose that a learning phase and utilization phase, partly exclusive, exist. The learning phase is induced during development, plausibly by depolarizing GABA$_A$ action, but could also potentially be induced later by descending control, for instance during sleep.

The learning phase starts with spontaneous activity in the reflex encoders causing, via the motoneurons, a muscle twitch. With respect to the skin, the effect of a muscle twitch in a limb, can be divided into two cases. Either the limb movement has a component along the direction of the normal to the skin which is greater than zero, or, a component that is less or equal to zero. For the skin area that has a negative normal the twitch is said to cause an unloading (Schouenborg & Weng, 1994). Strictly, true unloading would only occur if the skin area was in previous contact with an object or a surface. The next step in the learning sequel is that, the tactile fibers from the unloaded skin area change their activity, and relays this information to the multimodal SG interneurons, situated in the superficial dorsal horn. Next, this information will be broadcasted by the SG interneurons to the reflex encoders, that once started the whole process by their spontaneous activity. The final step in this learning scheme, is a Hebbian type modification of the strengths of the synapses that connect the SG interneurons to the reflex encoders.

The version of Hebbian learning we are using here has noteworthy deviations from the classical version. First, we are using Oja's rule (Oja, 1982) where the weights of the synapses are normalized to avoid biologically implausible growth of the synapses' strength. Second, and importantly, this learning scheme requires that the postsynaptic cell, the reflex encoder, fires first and then, when the sensory feedback arrives after the muscle twitch, the learning takes place. We therefore call this learning principle motor-directed somatosensory imprinting (MDSI). It represents post-pre pairing rather than pre-post pairing as is usually assumed in the CNS.

The utilization phase starts with a cessation, or a pronounced diminishing of spontaneous muscle twitches, and an increase in the threshold for mechanoreceptive fibers (Holmberg & Schouenborg, 1996). The timing approximately coincides with the increased expression of the neuronal specific K-Cl cotransporter, KCC2, which shifts GABA$_A$ channels to inhibitory action away from the immature excitatory action (Rivera et al., 1999).

Lastly, it should be noted that the proposed type of learning represents a cross-modality learning hypothesis, where tactile feedback is the teacher, but the user should be primarily nociceptive input, in order to give an purposeful withdrawal reflex in the adult animal.

When running simulations, based on the learning scheme and architecture described above, we used previously published data on the withdrawal patterns from five muscles (Schouenborg & Weng, 1994). At various stages during training, a correlation was calculated between the developing receptive field and the withdrawal pattern data for each muscle (Fig. 6C). At end of training, the correlation was typically found to be more than 90% and, importantly, was rather insensitive to twitching probability, learning rate, sensory noise and starting conditions. The training time (i.e. number of epochs) was determined based on the observed number of muscle twitches during the time of reflex adaptation (Waldenstam et al., 2002).

To further corroborate the hypothesis, that MDSI is taking place in sleep during development, experiments were performed on sleeping rat pups. In an experimental setting it could be shown that aberrant feedback, only given upon spontaneous tail twitches during sleep, could indeed cause an increase in movement error when noxious stimuli were applied to the tail after training period (Fig. 5A and A).

Through simulations, our architecture and self-organizing learning hypothesis have shown that a perceptron like architecture, i.e. without hidden layers, can faithfully and efficiently learn and execute the seemingly nonlinear transformation of the nociceptive withdrawal reflex. Other architectures and learning schemes, such as a feedforward Hebbian architecture (Fig. 6B and C), could not reproduce the experimental data.

Discussion

15 years of hindsight

It has been more than 15 years since the last of the Original papers presented in the thesis was published. Before deep diving into the respective papers, it is therefore natural to ask if the publications are still relevant today and if the results and conclusions seem to be correct, in the hindsight of 15 years of accumulated medical research. Although I think the short answer is clearly yes to both questions, it is worth to elaborate on this a bit more. The first two papers of this thesis are centered around a standard common investigative tool used in neurophysiology and brain research, the intracellular glass microelectrode. As such they are methodological papers, that has the primary outcome of understanding the limitations and implications of using microelectrode tools in neuroscience research. Although it is important and relevant to more thoroughly, as is done in paper I and II, elucidate the effects of, and construct a theory governing, the glass microelectrode, the primary purpose of these papers was to establish a method to assess transmembrane Cl^- homeostasis in a nerve cell preparation. But to answer the question of relevance and validity of Paper I and II, I believe, that to date, no other microelectrode measurements has been published in peer reviewed journals, that challenges or supersedes the results of Paper I, and the comprehensive theory presented in Paper II, is likely the correct one, although minor extensions could be made, for instance, in order to deal with multivalent ions or adding capacitive properties to the electrode as such.

For the investigations in Paper III and IV, centered around the intracellular Cl^- balance in a neuron, the information from Paper I and II on the Cl^- and K^+ leakage from microelectrode, was not only an essential data point, but actually used as one of the cornerstones of deducting quantitative data for the K-Cl cotransporter. Interestingly, the research on Cl^- homeostasis, which at the time of commencing the investigation of Paper III and IV was not in the scientific spotlight, has become a very rich and promising field of research. Although the precise numbers derived on the maximum transport rate of the K-Cl cotransporter or the lack of including other transporters into quantitative consideration, four main and important conclusions stay strong in the literature. First, the conclusions that K-Cl cotransporter indeed is the main transmembrane protein responsible for setting a low intracellular Cl^-.

Second, the conclusion, arrived at from simulations in Paper IV, that the cotransporter is almost silent at rest, due to working very close to its thermodynamic equilibrium point, defined as the point when the product of the intracellular concentrations of K^+ and Cl^- are identical to the product of the extracellular ditto. Third, as a consequence of "working close to its equilibrium", the K-Cl cotransporter becomes sensitive not only in changes of intracellular Cl^- but also very sensitive to changes in extracellular K^+. This mode, opposite to it's classical Cl^- extrusion mode, was shown in Paper III to be significant in volume and in Paper IV to be important in stabilizing the membrane excitability in high extracellular K^+. Fourth, the relative inability of the cotransporter, due to a nominal low intracellular Cl^- in neurons, to act as a defense against cellular swelling in response to hypoosmotic swelling. The fourth conclusion does not, however, contradict the important RVD function of the K-Cl cotransporter in the Cl^- loaded neuron, as is the case in the neonatal CNS, or in dynamic situation such as Cl^- loading during intense impulse firing with simultaneous inhibitory drive.

For the fifth paper presented here, there is an interesting connection to the other papers, besides the connection in terms of a dual computational and experimental approach to understanding neuroscience, in that the low expression of the K-Cl cotransporter in immature neurons is likely instrumental in enabling the tuning of the nociceptive withdrawal reflex. For the relevance and validity of this paper is true that the precise organization of the spinal cord is still under investigation and unfolding, but there is little doubt that the basic principle of using spontaneously active interneurons to initiate motor movements, from which the resulting sensory activation can be relayed back, and then correlated with the spontaneously active neurons is a strong and important principle. Spontaneously active interneurons are probably also probing and tuning other circuit in the CNS as part of a maturation and plasticity process.

Experiments on microelectrodes leading toward a theory for them (I)

This investigation was undertaken to understand how intracellular glass microelectrodes are affecting the very cells they are monitoring, and in particular to what extents Cl⁻ (and K⁺) is passed from 3.0 M KCl microelectrodes into the soma of neurons during intracellular work. The latter information was critically needed in order to understand and analyze the transmembrane flux of Cl⁻ in neurons impaled with glass microelectrodes.

The measurement of the Cl⁻ flux from the microelectrodes turned out to be tricky. Because the half-life of ^{38}Cl is short (37 min), the time window when the electrode experiments could be made at the nuclear reactor became narrow, and even hitting this time window, the residual activity of ^{38}Cl at the time of analysis were already quite small. Nevertheless, in resting conditions (zero current injection), a background leakage of -3.7 nA for Cl⁻ could be calculated and, in independent measurements, +3.8 nA for K⁺. The similarity of values speaks to the reasonable validity of these difficult measurements, since at rest, the currents need to add up to zero for reasons of macroscopic electroneutrality (in the absence of any other current carriers in relevant amounts). Also, the approximate values we found are not at variance with other ^{42}K efflux experiments (Fromm and Schultz, 1981), after adjusting for electrode resistance and electrode filling concentrations.

From our experiments (Paper I) it also became evident that during current injection, K⁺ is carrying the bulk of charge across the electrode opening. This fits nicely with the rectification properties of these electrodes as will be discussed later. Judging by the experimental data, it appears that K⁺ is carrying almost 80 percent of the charge for positive currents (in the direction out from the electrode), and similar for negative currents. This result turns out to be somewhat different from the simulations of the microelectrode model (Paper II), where K⁺ is carrying two thirds of the charge during positive currents and little more than half of the charge during negative currents (Fig. 15). This will be addressed fuller below (in Paper II).
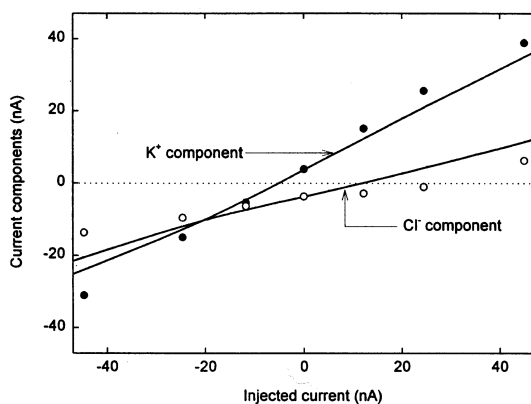

Figure 15. Simulated K⁺ and Cl⁻ current components as part of total electrode-injected (transelectrode) currents. The horizontal dotted lines mark the level of zero transelectrode current. The open and closed circles represent experimental observations in Paper I.

In our measurements the size of the tip potential was similar to other studies on beveled microelectrodes (Isenberg, 1979) and we also found that the tip potential is decreasing with the size of the electrode opening. This is supporting the idea that an electrical double layer, due to negative surface charges on the glass inner surface, exists in the glass microelectrode (Adrian, 1956; Schanne et al.,1968). Such as electrical double layer would imply that the K^+ ions have access to the full cross-sectional area of the electrode for diffusion, but that Cl ions only have access to the cross-sectional area minus the thickness of the double layer. In essence, the effective "permeability" would differ for the Cl^- and K^+ ions, and a tip potential would be the outcome.

For the characterization of the rectification properties of the microelectrodes, is it interesting to note that the degree of rectification is reduced towards zero when the electrolyte solution inside and outside the microelectrode becomes equal (Fig. 10A and Fig. 10B). This could support the observation by Tayler (1953), who first ascribed the rectification to electroosmosis, since with equal concentrations inside and outside the electrode, electroosmosis cannot change the distribution of the current carriers; K^+ and Cl^- ions (more details in Discussion section of Paper II). More generally, it thus seems that the various electrode properties are determined by electrodiffusion, acting on the dissolved charged particles, and electroosmosis, acting on the water solution inside the electrode.

Explaining microelectrodes by simulations and guiding their usage (II)

In order (a) to understand how microelectrodes influence the very cell they are studying, such as the various artifact that can be expected during intracellular work, and (b) for potentially designing new microelectrodes, tailored for specific experimental needs, it seems justified to develop a comprehensive mathematical model of the intracellular glass microelectrode. Here we will discuss some of the features of such a model and run additional simulations to better grasp intracellular microelectrode work.

Importantly, the glass microelectrode model we construct here, differs from other attempts in characterizing electrodes by employing only two fundamental equations, both of which, from the results of Paper I, clearly seem to be at work in the glass microelectrode system. Also, the model is virtually without adjustments, only the parameters that are hard to directly measure, the zeta potential ξ, and Debye lengths

δ, are adjusted to fit the data set. The adjusted values were found to match literature data.

From tests performed on the model (Fig. 10A) it is clear that the model is reproducing experimental data in a convincing manner and we decided to adopt it as a microelectrode theory and simulate the electrode under other model conditions.

For instance, in model simulations, it is possible to study the electrodes current rectification with a space and time resolution that is not readily available in experiments. Doing so, it becomes evident from Fig. 16A that electrolyte concentration shifts up or down the electrode's tip portion is the true cause of rectification. During positive currents pulses the electrolyte concentration profile becomes very steep and condensed to the absolute tip of the electrode, and during negative currents the concentration profile is flattened out. The change in the electrolyte's concentration gradient $\frac{d[X]}{dx}$, is in the order of a factor 10, and in the vicinity of the electrode opening, the concentration $[X]$, is also changed by a factor of the order 10. Since both the electrodiffusive current (Eq. 5) and the electroosmotic current (Eq. 7) is linearly dependent on $\frac{d[X]}{dx}$ and $[X]$ respectively, the total current, which is the sum of the two, will also be a factor of 10 larger, other factors equal.

To illustrate this, it is worth studying concentration shifts in the electrode tip region with high time resolution. By applying a -20 nA current pulse, it is seen that already after 10 ms the concentration profile has changed more than halfway to its steady state profile (Fig. 16B). In full analogy, 10 ms after applying any current pulse, the corresponding IV curve is more than halfway towards its steady state rectification (Fig. 10A).
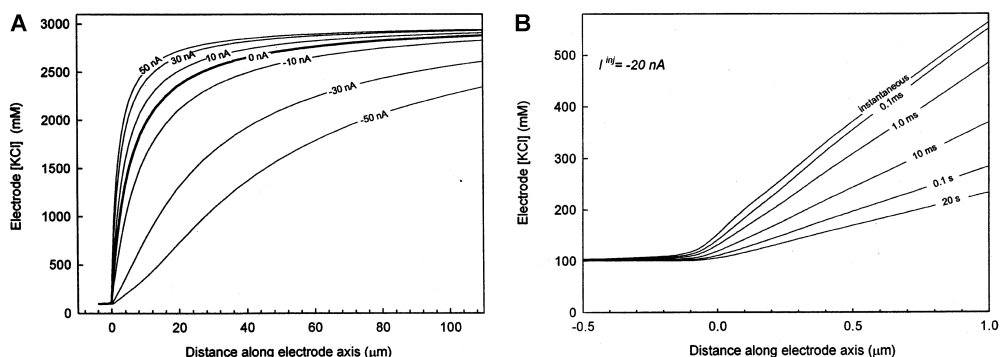

Figure 16. Simulations of electrode [KCl] curves in space and time at various transelectrode currents.
A, Steady state relationships between distance along the electrode axis and [KCl] at various transelectrode currents. **B**, Relationships between distance along the electrode axis and [KCl] at various times from onset of a -20 nA transelectrode current.

Going further back in the causality chain, the reason for the asymmetric concentration shifts is the electroosmotic volume flow of electrolyte up and down the electrode shaft. If the immersion solution and the electrode filling solution is the same, volume flows will have no effect (Fig. 10D) since the concentration profiles will remain the same. Also, putting the zeta potential to zero, no current rectification can be created (Fig. 17), since no volume flow takes place.
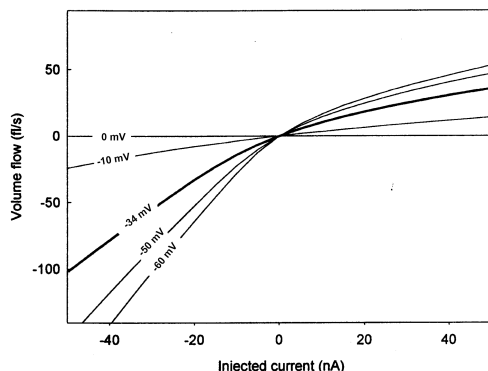

Figure 17. Effects of varying the zeta potential on electrode properties. Steady state relationships between electrode-injected current and volume flow at various zeta potentials, as indicated. The thick curves represent standard conditions with ζ = -34 mV.

From Fig. 17 it is seen that to accomplish high volume flows, with the purpose of solute injection, a large zeta potential is desired. Combining a large zeta with a low concentration of carrier ions will give the best results. A volume flow of more than +100 fl/s can be created with a zeta potential of -60 mV, filling solution of 3.0 M KCl at a current of +30 nA.

In the literature it has been noted that the practice of using 3.0 M KCl microelectrodes should be restricted to large cells or cells equipped with an efficient Cl^- and K^+ extrusion machinery, since the leakage is otherwise likely to distort the cell membrane potential, change the cell volume or even cause cell death (Geisler et al., 1972; Fromm and Schultz, 1981; Blatt and Slayman,1983). From model simulation it is easy to concur with these recommendations. It is seen that the passive leakage of K^+ and Cl^- is directly proportional to the concentration difference between the filling solution and the immersion solution (Fig. 11C), so employing 0.5 M KCl instead of 3.0 M KCl will give a 7-fold decrease in passive leakage, but only an approximately 3-fold increase in typical electrode resistance. The rectification will also be significantly reduced (Fig. 10C) and the tip potential is predicted to be unaffected by the concentration change to 0.5 M KCl in the filling solution (Fig. 11D).

Contemplating the extraordinary ability of our simulations to reproduce experimental data, and to help explain in some detail the root cause behind various electrode properties, it is disturbing that the fit to experimental data for the partitioning of K^+ and Cl^- during during current injection is, in comparison, relatively poor (Fig. 15). It seems that the likely cause is as follows. When assessing

a flux of a substance across an imaginary surface from one space to another, it is the net flux we are trying to measure, in our case how much net Cl^- or K^+ are entering of leaving the electrode. In reality, across any interface in the electrode or any other interface, the flux of Cl^- from one side to another is orders of magnitudes larger than the net flux of Cl^- across that interface. Our measurement, relying on radiotracers ("hot" KCl) only on the inside of the electrode is therefore only measuring Cl^- or K^+ that emanated from the inside of electrode and not any Cl^- or K^+ that emanated from the outside. The reason why our measurements still are somewhat accurate is that the difference in concentration of the immersion solution ("hot" KCl) and the filling solution is a factor of 30. Hence, the bulk of electrodiffusion will be in the outward direction and some of the electrodiffusion going back into the electrode will actually be consisting of ions originating from the inside of the electrode and partly offset our methodological problem of measuring a flux across an interface, starting with particles on only one side of an interface.

With electroosmotic flow another dynamic is entering the picture. During positive currents, electrolyte will be driven out of the electrode, and there will be only a small overestimation of K^+ since now a larger part of the K^+ electrodiffusing back are $^{42}K^+$ (hot K^+), due to the abundance of $^{42}K^+$ just outside the electrode tip from the electroosmotic flow. During negative currents on the other hand, immersion solution electrolyte will be sucked into the electrode while Cl ions are struggling in the headwind to carry their charge out from the electrode. Under these conditions, a substantial part of the Cl ions leaving the electrode will be from the cold Cl^- and thus not accounted for in our set-up. Therefore, an underestimation of Cl^- efflux during negative currents could be significant, despite the low concentration of Cl^- (and K^+) in the cold immersion solution.

With this background it is reasonable to assume that the simulations are correct and that the experiments yielded a small overestimation of the K^+ carried currents during positive currents, and a larger underestimation of Cl^- carried currents during negative current, which is precisely what the data indicate (Fig 15). With a similar train of reasoning, the passive leakage of ±3.8 nA in our experiments is likely overestimated, and more correct value is the simulation result of ±3.5 nA.

In this Paper II we have shown that the glass microelectrode's electrical and electrochemical properties can be explained by the laws of electrodiffusion and electroosmosis with prior knowledge of the geometric configuration of the tip region (last mm), density of fixed charges on the inner wall and the concentration of the filling and immersion solution only.

The model will also be used to identify the chloride balance and dynamics in a neuron (Paper III and Paper IV).

Transmembrane Cl⁻ balance in experiments and simulations (III, IV)

Identified Cl⁻ transporters

Chloride ion concentration gradients play key roles in neurons for functions such as inhibition, excitability and plasticity. How chloride ions are regulated and how they cross the plasma membrane by carriers and channels are therefore fundamental to understanding these cells. In the present study we could show that an electroneutral K-Cl cotransporter does exists in our cell, and that it is likely the main Cl⁻ extrusion mechanism, and as such, responsible for setting the Cl⁻ equilibrium potential lower than the membrane potential, enabling efficient inhibition. We could further show that it is capable of reversing its direction in high extracellular K^+ and that it is blocked by furosemide, SITS and DIDS, and is activated by NEM.

The isoform of the K-Cl cotransporter that we have identified could be related to the KCC2 isoform found abundantly in mammalian CNS (Payne, 1997; Payne et al., 2003). As the principal agent for achieving low intracellular Cl⁻ in neurons, KCC2 is constitutively active. Other isoforms KCC1, KCC3 and KCC4 are usually silent unless triggered by cellular events, the most classical being intracellular swelling. Under the standard experimental protocol in this study, cells are impaled with a 3.0 M KCl filled microelectrode, so it is reasonable to assume that some degree of cell swelling does exist due to leakage of KCl electrolyte into the cell. This leakage is estimated to increase the intracellular Cl⁻ concentration by around 30 mM. An equal increase in the number of K^+ ions is expected, but a smaller increase in concentration terms, due to the high pre-swelling K^+ concentration, which is diluted more in absolute terms upon swelling. The increase in osmoles, estimated this way, corresponds to around 8% of the total osmoles in the cell and could cause a swelling of around 8%. Thus, it is possible that, to the extent that two or more isoforms of the K-Cl cotransporter exists in the lobster stretch receptor neuron, more than one isoform have been lumped together in our investigation.

Although we could not identify a Na-K-2Cl cotransporter under our experimental conditions, it is nevertheless likely that it exists in the preparation. From the literature it is evident that the Na-K-2Cl cotransporter is evolutionary strongly conserved and abundant in all tissue, including neurons, and has also been identified in other crustaceans (Towle & Weihrauch, 2001). Being an efficient and fundamental defense mechanism against cell shrinkage by hyperosmotic shock, it is probably an indispensable tool in any cell. It is therefore probable that a Na-K-2Cl cotransporter does exist in our neuron as well, despite our failure to identify it. However, Na-K-2Cl cotransporter, along with several isoforms of K-Cl cotransporter (KCC1, KCC3 and KCC4) are nominally silent in cells except when

triggered by external events. It is therefore not surprising that we could not detect any ion concentration changes during our attempt to block it since cell shrinkage was not at hand, rather cell swelling due to KCl loading from the microelectrode.

Cell shrinkage or cell swelling events typically lead to phosphorylation or dephosphorylation of NKCCs and KCCs respectively. To trigger the phosphorylation and activate NKCCs a hyperosmotic shock is a biologically relevant method. NKCC will then serve as a Regulatory Volume Increase mechanism in response to cell shrinkage. In doing so, it will transport one Na^+, one K^+ and two Cl^- into the cell per cycle, hence the abbreviation Na-K-2Cl. During our experiments, raising extracellular K^+ and Cl^- by 35 mM to 40 and 448 mM respectively, an 8.5% increase in extracellular osmolality is achieved, which could potentially trigger the Na-K-2Cl cotransporter. However, since our cells are impaled with a 3.0 M KCl microelectrode the intracellular Cl^- (and similar for K^+ for electroneutrality reasons) is around 30 mM higher than in unimpaled cells. Therefore, the hyperosmolar event is, in reality, just resetting the osmolality between the cell interior and exterior, and therefore, there are no clear reasons to assume that Na-K-2Cl becomes activated. Further reasons to believe that our experiments with high K^+ (and Cl^-) were primarily dealing with K-Cl cotransporter, and not the Na-K-2Cl, are that no changes could be detected in intracellular Na^+ following applications of high extracellular KCl, but a profound increase in intracellular KCl.

Functions of the K-Cl cotransporter

The two main functions of the K-Cl cotransporter, each with implications on conditions in the CNS, could be summarized as, one, setting the intracellular Cl^- concentration below its electrochemical equilibrium concentration and, two, to achieve KCl flux (primarily outward) in response to cell volume changes (primarily swelling events). In addition, we find evidence for a potential important functional role for the cotransporter in situations of elevated extracellular K^+, where the transport direction would reverse, and the cotransporter would transport KCl inwards.

For the first task, while it is established in the literature the importance of KCl cotransport for achieving a low intracellular Cl^- it has not been simulated in a neuron before. In Paper IV we simulate the effect of the K-Cl cotransporter on a native neuron by first unimpaling our mathematical neuron model. This is accomplished by setting the impalement permeability to zero and the electrode KCl leakage to zero. After readjustments of currents, ions concentrations, and membrane potential, the model cell reaches a new equilibrium. The end result is a hyperpolarizing of around 10 mV (to -74.3 mV), and a shift in intracellular Cl^- concentration from 46.7 mM down to 17.4 mM. This gives a Cl^- Nernst potential of -79.5 mV, ensuring an

efficiently working inhibitory machinery, some 5 mV lower than the membrane potential. It is worth noticing the very small current produced by the K-Cl cotransporter at rest, and therefore that relatively little energy needs to be spent (ultimately by means of the Na/K pump) to keep this homeostasis. The small current further implies that the cotransporter is operating close to its thermodynamic equilibrium, implying that a moderate absolute change in extracellular K^+ could reverse its direction. Repeating the procedure of unimpalement, but with the K-Cl cotransporter blocked, yields as expected, a Nernst potential for Cl^- identical to the membrane potential.

From our experiments, it also seems clear that the K-Cl cotransporter can give rise to large outward fluxes of KCl, as must be the case, for instance, during impalement with 3.0 M KCl glass microelectrodes, where significant amounts of KCl leaks into the cell. A biologically more realistic situation generating an intracellular Cl^- load would be during intense impulse firing with simultaneous inhibitory drive. Under these circumstances large inward chloride flows are expected since (a) the Cl^- permeability during GABA stimuli is 200-300 times larger than the permeabilities of other non-voltage gated channels, (b) the electrical driving force for Cl^- at the peak of the action potential will be around 100 mV and (c) extracellular Cl^- concentration is 400 mM thus supplying plenty of carrier ions. The subsequent increase in submembrane intracellular Cl^- concentration (Fåhraeus & Grampp, 1993) will drastically change the equilibrium potential for Cl^- and cause GABA stimuli to be excitatory (and shunting). A large transport capacity for K-Cl cotransporter should decrease the peak Cl^- increase and speed up the recovery to maintain homeostatic excitability.

In Paper IV we simulate, on the full receptor neuron model, including the voltage gated channels, intense impulse firing with a simultaneous inhibitory drive. This is done by opening a non-specific channel for Na^+ and K^+ emulating a stretch activated channel for 5 seconds while simultaneously opening up a $GABA_A$ permeability of 300-fold the magnitude of the resting cells Cl^- permeability, the latter opened for 3 ms at 5-10 Hz. In order to mimic conditions in submembrane space (Fåhraeus & Grampp, 1993), or in dendrites space, the cell volume was set to 1% of the normal. Doing so (Fig. 18A), it is seen that chloride concentration is increasing by more than 2 mM per second and after just one burst of 5 seconds activity a 10 mM increase is observed. Although the KCl current never achieves high current strengths in these short experiments, mainly due to simultaneous depletion of intracellular K^+, the difference when repeating the experiments with a KCl block is evident, an increase in intracellular chloride is large and persists for minutes, basically rendering the inhibition dysfunctional for a long time. We can therefore with some assurance conclude that the K-Cl cotransporter plays a crucial role not only in the setting of low intracellular chloride in the resting cell but also in the rapid restoration in cell dynamics.
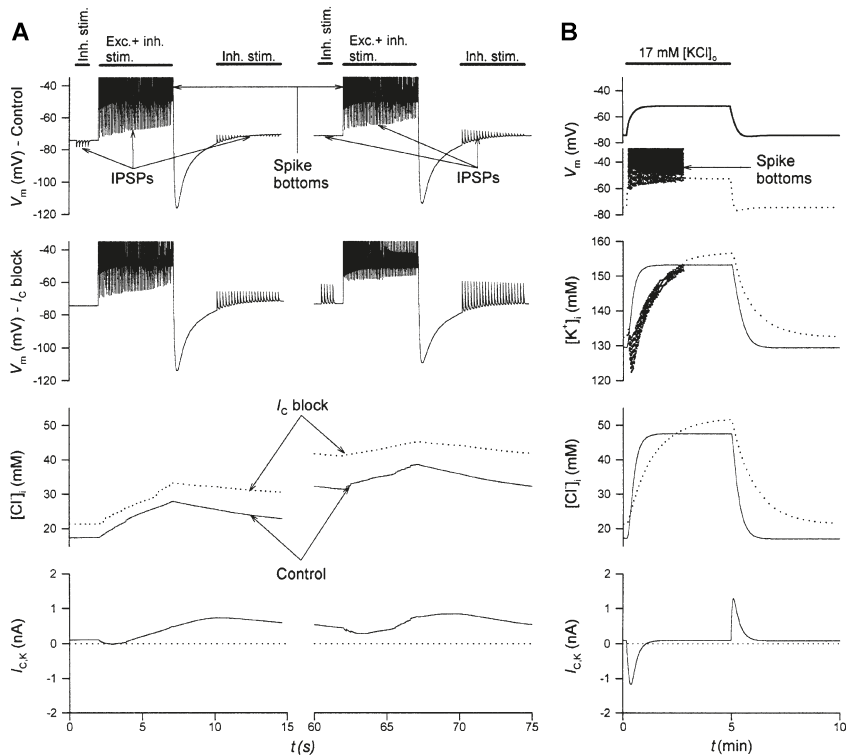
Figure 18. Model simulations on an unimpaled cell, whose volume was set to one-hundredth of its standard value (to mimic submembrane or dendrite space).

A, Effect of excitatory and/or inhibitory stimulation (indicated by horizontal bars above top panels) on membrane potential, V_m; intracellular Cl⁻ concentration, $[Cl^-]_i$; and K⁺- carried K–Cl cotransporter current, $I_{C,K}$; before and after blocking the K–Cl cotransporter completely (marked by Control or I_c block) Excitatory and inhibitory stimulation was achieved by either a continuous influx of Na⁺ and outflux of K⁺ (simulating a square pulse of stretch stimulation), and by repetitive pulses (3 ms, at 10 or 5 Hz) of a 300-fold increase in Cl⁻ permeability (simulating opening of GABA$_A$ channel, eliciting post-synaptic potentials, IPSPs). In all panels, the left parts show events during the first, and the right parts events during the last of five successive cycles of stimulation. **B,** Effect of shifting the K⁺ concentration from 5.0 (standard) to 17.0 mM (horizontal bar above the top panel) on the membrane voltage, V_m; intracellular K⁺ and Cl⁻ concentrations, $[K^+]_i$ and $[Cl^-]_i$; and the K⁺-carried K–Cl cotransporter current, $I_{C,K}$; before (solid lines in all panels) and after (dotted lines in all panels) blocking the K–Cl cotransporter completely. In the upper panels of both A and B only the lowest parts of action potentials are shown.

In another experiment (Paper III), by raising extracellular K⁺ to 40 mM, we could demonstrate that the K-Cl cotransporter can change direction and achieve large inward fluxes of KCl. Elevated extracellular K⁺ is expected to occur in at least two biologically relevant scenarios. First, during feeding where K⁺ of intracellular origin from the prey is taken up in extracellular space of our animal, and second, during intense impulse firing. In intense firing, extracellular K⁺ will rise significantly due to the limited pericellular space around neurons to harbor the outward K⁺ flux from the voltage gated K channels. Since K⁺ channels are the dominating channels for setting the resting membrane potential this leads to a general depolarization and altered sensitivity for new excitatory synaptic stimuli.

As such, it is a severe disturbance of the information processing and excitability and needs to be taken care of. Although multiple mechanisms are relevant in restoring extracellular K^+ homeostasis, such as the Na-K pump, a K-Cl cotransporter could clearly be one key element in this, transporting K^+ (and Cl^-) across the membrane to the cell interior.

In order to simulate this experimental setup in our mathematical model of the receptor neuron (Paper IV), we expose the cell to elevated extracellular K^+, yielding a total of 17 mM (Fig. 18B). Again, we use a cell with radically reduced volume to mimic a submembrane space or a dendrite tree volume. In these conditions, the K-Cl cotransporter is indeed accomplishing a rapid inward shift of K^+, increasing the intracellular concentration, and thereby, facilitating the partial restoration of the K^+ concentration gradient and the corresponding Nernst potential. In this example, the small increase in membrane polarization that follows enables the cell to stay clear from inappropriately triggered action potentials, whereas a cell with blocked K-Cl cotransporter is inappropriately bursting for minutes. From both our experiments and simulations it therefore seems likely that the cotransporter, in addition to establishing a favorable Cl^- gradient for synaptic inhibition, is also involved in mitigating harmful increases in pericellular/extracellular K^+ by reversing its transport direction, even if this means an increase of intracellular Cl^-. It is worth noticing that in our model rather small absolute changes in the concentration of extracellular K^+ will cause a reversal of the transporter direction, due to the assumption that the transport direction is determined by the difference in the product of the concentrations, intracellularly and extracellularly, only. A change of extracellular potassium from 5 to 10 millimole, for instance, will double the extracellular product, illustrating the potential efficacy of this situation (see also Payne, 1997).

For cell volume regulation, particularly in Regulatory Volume Decrease (RVD) following cell swelling K-Cl cotransporters play a key role (Lauf et al., 1992). However, for neurons, where the nominal intracellular chloride concentration is low compared to non-neuronal cells, the efficacy of volume decrease by extrusion of KCl in response to cell swelling from hypotonic shock, is limited. To model extracellular osmotic changes, we simulated various settings of extracellular KCl (Fig. 19). From these experiments two things are clear. First, without a functioning K-Cl cotransporter the cell has little defense combatting changes in extracellular KCl, the cell volume will decrease (or increase) and stay like that for hours in our model cell. Secondly, even with a functioning K-Cl cotransporter, that does respond and mitigates the cell volume decrease and cell volume increase, it is evident that other components are needed in an efficient cell volume homeostasis control system. For instance, in our experiments, the RVD accomplished by the K-Cl cotransporter gives rise to a troublesome overshoot in cell volume, further exacerbated on return to nominal extracellular [KCl].

The three most obvious candidates lacking, for a more functional volume homeostasis machinery, are a Na-K-2Cl cotransporter for Regulatory Volume Increase (RVI), volume and/or ionic strength sensing proteins and purposeful feedback loops for turning cotransporters (KCCs and NKCCs) on and off by dephosphorylation and phosphorylation respectively. The membrane-bound serine-threonine phosphatases PP1 and PP2A have been identified as responsible for the activation of KCCs by dephosphorylation, where PP1 is thought to be ionic strength sensing and PP2A cell swelling sensing (Bize et. al., 1999). The WNK-SPAK/OSR1 signaling cascade is responsible for inactivation (by means of phosphorylation) of all four KCCs and at the same time for the activation (by phosphorylation) of NKCC1 and NKCC2 (Kahle et al, 2015; de los Heros et. al., 2014), indicating that NKCCs do not normally operate simultaneously as KCCs.

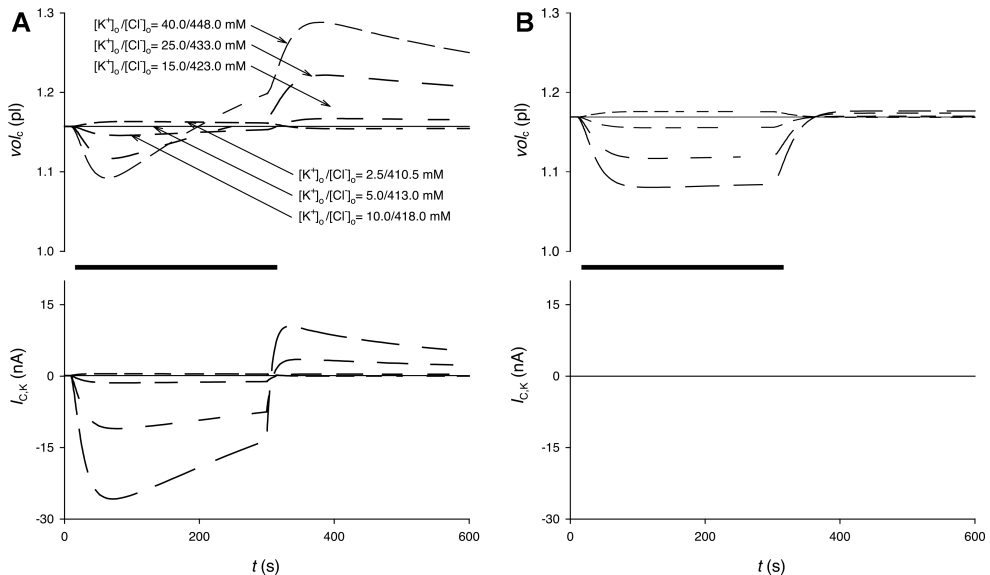For a full model of volume regulation also volume sensing channels such as VRAC would be needed.

Figure 19. Model simulations of unimpaled cells on cell volume and K–Cl cotransport activity in different extracellular [KCl].
A, Changes in cell volume, vol_c (upper panel), and K^+-carried K–Cl cotransporter current, $I_{C,K}$ (lower panel) caused by changes in extracellular K^+/Cl^- concentrations, $[K^+]_o/[Cl^-]_o$, with 5.0/413.0mM being baseline. **B,** Changes in cell volume (upper panel), in a cell with a blocked K–Cl cotransporter, with the same concentration changes as in A.

Intracellular Cl⁻, maturation and learning in the CNS

It is well established that during the maturation of the mammalian nervous system an interesting change occur, where the NKCC1 is downregulated and KCC2 is upregulated, with a reciprocal shift in intracellular Cl⁻ from higher to lower concentration (Rivera et al., 1999; Kahle et al., 2015; Nardou et al., 2013). This is the reason why GABA initially acts as an excitatory transmitter substance and later as an inhibitory transmitter substance in the adult animal. Philosophically, it could be argued that if all units in a system are inhibiting each other it is hard to discern the total connectivity in the network, since signals will not be transmitted beyond the postsynaptic neuron. For a network to efficiently organize itself it is important to understand the circuitry, and then excitatory post synaptic potentials, especially in combination with spontaneously active neurons, will have a better chance of probing the gross connectivity. This could be especially true if test pulses are sent out, in order to see what comes back to the same neuron, as could be the case in the spinal cord for the nociceptive withdrawal reflex (Paper V).

The switch from depolarizing GABA action to inhibitory, takes place at approximately the same time as tuning of motor skills start to occur in mice (Rivera et al., 1999; Holmberg & Schouenborg, 1996a). In the immature brain many glutamatergic synapses are inactive ("silent") since at that stage NMDA channels are the dominant receptor for glutamate, and the NMDA receptor will not pass current unless Mg^{++} is unblocking the NMDA channel by means of membrane depolarization (Isaac et. al. 1997). Further, for NMDA dependent LTP to start take place, AMPA receptors need to be inserted into the postsynaptic membrane, but can only do so if current flows through the NMDA channel. Strong evidence is now suggest that depolarizing GABA action is necessary for LTP to start occurring at these glutamatergic synapses (Leinekugel et. al., 1997; Wang & Kriegstein, 2008). Once the unmasking of the AMPA receptor is achieved by depolarizing GABA, the tuning of the synapse by LTP or LTD does not require depolarizing GABA.

Since the shift in GABA action from depolarizing to hyperpolarizing is taking place at different times in different parts of the CNS, it is tempting to speculate that specific network layers, or Hebbian input-output pairing opportunities, are tuned, or paired, at different times in the CNS, enabling easier optimization than a multi-layered network would (Rivera et al., 1999). Another implication of the unmasking of AMPA receptors by depolarizing GABA, is that only neurons with a dual inhibitory and excitatory convergence are selected for NMDA dependent synaptic plasticity, perhaps also requiring a proximity within the neuron of the $GABA_A$ receptor and the NMDA receptor. This has interesting implication for the network architecture of the CNS and for the potential for $GABA_A$ receptors to efficiently modulate the excitability of a neuron or even of individual excitatory synapses.

K-Cl cotransporter and implications for neuropathologies

Clearly intracellular Cl⁻ is responsible for the size of the (Cl⁻ mediated) inhibitory response on a postsynaptic cell level and thereby in setting the excitability of individual cells, neural circuits and of the CNS. It is thus not surprising that disturbances in the Cl⁻ homeostasis and dynamic regulation give rise to neuropathologies. Some of the best studied examples associated with elevated intracellular Cl⁻ and impaired KCC2 function are epilepsy (Delpire, 2000; Cohen, 2002; Deisz et al, 2011) and neuropathic pain (Coull et al., 2003) but the growing list includes autism spectrum disorders (Ben-Ari, 2015), Huntington's and Parkinsons's disease (Dargaeia et al. 2018, Braithwaite et. al. 2012), motor spasticity and schizophrenia.

In childhood, a mutation in KCC2 has also been identified, which leads to a severely impacted ability to extrude Cl⁻ and a debilitating juvenile epilepsy (Stödberg et a., 2015). Other childhood Cl⁻ pathologies are associated with disturbed timing in the shift from high intracellular Cl⁻, through NKCC1 dominated expression, to low intracellular Cl⁻, through increased KCC2 expression (Kahle et al, 2015). In many cases, adult and juvenile, the diseases seem to be associated with a decreased expression of KCC2, following trauma or inflammation (Ronen et al., 1999; Payne, 1997; Payne et al 2003). Microglia, the innate immune system of the CNS, will migrate to regions of neuronal damage and death and start a scarring and healing processes. Interestingly, microglia secretes BDNF which is now believed to be one of the key factors in the downregulation of the KCC2 expression of neurons after trauma. Therefore, trauma often cause neurons to de-differentiate to the immature state of the developing CNS, probably regaining better plasticity, sprouting and retargeting capabilities (Payne et al., 2003). This seems to be one major factor behind neurologic pain for patients with spinal cord injury and for epilepsy in patient after neurosurgery in CNS or after hemorrhage and asphyxia.

Taken together, targeting KCC2 or the balance between NKCC1 and KCC2 is therefore a biologically plausible pharmacological target with a large unmet medical need. Already, existing drugs such as bumetanide have shown that (partially) blocking the Na-K-2Cl cotransporter can be advantageous in Autism Spectrum Disorders, Parkinson's disease and epilepsy (Ben-Ari, 2017). However, manipulating the system of Cl⁻ homeostasis is unlikely to be straightforward, since turning on the KCC2 in Cl⁻ loaded neurons of the CNS, will initially likely cause a rise in extracellular K^+, and a subsequent spreading depression prone to worsen epilepsy. This may be the reason for the somewhat conflicting data on the merits of turning on or off the KCC2 and in blocking the NKCC1 cotransporter in models of epilepsy (Nardou et al., 2009, Nardou et al., 2013). A computational model incorporating a realistic extracellular and intracellular geometry in the CNS, including glia and neurons, could probably shed light on the parameter landscape

governing the outcome of various settings of cotransporters, inhibitory/excitatory drive, channel populations, pH machinery, and not least the density of Na-K pumps, driving the system. It is likely that such experiments will show that different measures are needed depending on starting conditions, and on desired outcome. However, as a general remark, with a KCC2 operating near its thermodynamic equilibrium point in the healthy CNS, the benefits with a highly expressed and functional KCC2 should be the preferred state in the adult CNS and could have positive implication on a spectrum of neuropathologies and possibly also aging. Having said that, it is clear that Cl⁻ is dynamically regulated and may rise or fall as part of normal cycle also in the adult CNS, for instance in circadian rhythm regulation (Delpire, 2000; Wagner et al., 1997).

Learning the 3D body shapes by spontaneous muscle twitches (V)

In this work we show that spontaneous motor-initiated twitches of single muscles can serve as an ideal strategy for the CNS to lay down the relationships between 3D body surface movements and muscle activity. We call this the motor directed somatosensory imprinting (MDSI) principle which may also have imperative relevance for other reflexes and somatosensory imprinting in general.

We also show that the nociceptive withdrawal reflex could be accurately constructed as the additive action of individual muscle movements and hence it is well implemented in a perceptron like manner and does not require a network consisting of several hidden layers.

For the biological and molecular bases of MDSI it is interesting to note that the pivotal spontaneous muscle twitches are ubiquitous during development (Blumberg & Lucas, 1994) and common also during sleep in adult mammals. It is also well known that neurons in the spinal cord undergoes changes in their patterns of excitability during development. One possibility is that the reflex encoders, through Ca^{++} plateau potentials initiated by depolarizing $GABA_A$ action (Ben-Ari et al., 1997; Ben-Ari & Spitzer, 2010) during sleep (Frank et al., 2001), cause the muscle twitches and open up the cell for post-presynaptic correlation-based learning. For channels responsible for this synaptic plasticity it is likely that NMDA channels and AMPA channels through LTP mechanisms are at work (Ben-Ari & Spitzer, 2010). While the withdrawal reflex can be elicited both by noxious stimuli and tactile, it is noteworthy that the threshold for tactile input seem to undergo developmental changes (Holmberg & Schouenborg, 1996a), maybe because the reflex circuitry goes into to an adult mode where adjustments are less frequent and needed, and where primarily noxious stimuli should elicit the reflex.

Importantly, the assumption with tactile input giving an inhibitory postsynaptic activity on SG interneurons is not import for the MDSI principle. If we instead assume that tactile fibers gives excitatory postsynaptic potentials on SG neurons, we have to replace the learning rate η with a negative learning rate $-\eta$ and the results would be equivalent. This latter scheme would represent an LTD type learning. The key factor for learning to take place is the correlation (positive or negative) between spontaneous activity in the spinal cord, causing a muscle twitch, and sensory feedback. The learning hypothesis has an obvious advantage in that it brings together a number of observations into a comprehensive and extremely efficient tuning algorithm.

A more quiescent spinal circuits is probably organized and adjusted by the same principle, namely the inhibitory reflex system responsible for inhibition of the withdrawal reflex (Weng & Schouenborg, 1996). This reflex, with receptive fields for a certain muscle corresponding to the movement direction towards the skin caused by the same muscle, can be seen as inverse of the withdrawal reflex, which has receptive fields corresponding the movement away from the same skin area. The inhibitory reflex is needed to avoid that while trying to move away from a noxious stimulus, the movement itself does not cause damage. A putative architecture could be almost identical to the withdrawal reflex but would most likely need to feed to other premotoneurons (reflex encoders), yet to be identified in the spinal cord.

In conclusion, it seems likely that the spontaneous muscle twitches that are dominating the motor behavior in fetuses and neonatal animals during sleep, are in fact the foundation for self-organizing all the reflexes that are performed at the spinal cord level, for example the Golgi tendon reflex, muscle spindle reflex, cross extensor reflex and the reciprocal inhibition reflex mentioned above. Lastly, the concept of test pulses by spontaneously active neurons in combination with depolarizing GABA, may be one of several cornerstone strategies for also higher centers of the neonatal CNS to self-organize by discovering, expanding and tuning the innate connectivity.

References

Adrian, R. H. (1956). The effect of internal and external potassium concentration on the membrane potential of frog muscle. J. Physiol. 133: 631-658.

Agin, D. & Holtzman, D. (1966). Glass microelectrodes: The origin and elimination of tip potentials. Nature 211: 1194-1195.

Aickin, C. C. (1994). Regulation of intracellular pH in the smooth muscle of guinea-pig ureter: HCO_3^- dependence. J. Physiol 479.2: pp. 317-329.

Alvarez-Leefman, F.J. (1990). Intracellular Cl^- regulation and synaptic inhibition in vertebrate and invertebrate neurons. In: F. J. Alvarez-Leefmans & J. M. Russel (eds) Chloride Channels and Carriers in Nerve, Muscle and Glial Cells, pp. 109-158. Plenum Press, New York and London.

Altamirano, A. A., Breitwieser, G. E. & Russell, J. M. (1995). Effects of okadaic acid and intracellular Cl^- on Na^+-K^+-Cl^- cotransport. Am J Physiol 269, C878-C883.

Begenisich, T., & Melvin, J.E. (1998). Regulation of Chloride Channels in Secretory Epithelia. J. Membrane Biol. 163, 77–85.

Ben-Ari, Y., Khazipov, R., Leinekugel, X., Caillard, O. & Gaiarsa, J.-L. (1997). $GABA_A$, NMDA and AMPA receptors: a developmentally regulated 'ménage à trois'. Trends Neurosci. 20, 523–529.

Ben-Ari, Y. & Spitzer, N. C. (2010). Phenotypic checkpoints regulate neuronal development Trends in Neurosciences Vol. 33 pp. 485-492.

Ben-Ari, Y. (2015). Is birth a critical period in the pathogenesis of autism spectrum disorders? Nature reviews: Neuroscience Vol 16 pp. 498-505.

Ben-Ari, Y. (2017). NKCC1 Chloride Importer Antagonists Attenuate Many Neurological and Psychiatric Disorders. Trends in Neurosciences, Vol. 40, No. 9, pp. 536-554.

Bize, I., Guvenc, B., Robb, A., Buchbinder, G. & Brugnara, C. (1999). Serine/threonine protein phosphatases and regulation of K-Cl cotransport in human erythrocytes. Am. J. Physiol. 277: C926–C936.

Blatt, M. R. & Slayman, C. L. (1983). KCl leakage from microelectrodes and its impact on the membrane parameters of a nonexcitable cell. J. Mebr. Biol. 72: 223-234.

Bliss, T. V. & Lomo, T. (1973). Long-lasting potentiation of synaptic transmission in the dentate area of the anaesthetized rabbit following stimulation of the perforant path. J Physiol Vol. 232, pp. 331-56.

Blumberg, M. S. & Lucas, D. E. (1994). Dual mechanisms of twitching during sleep in neonatal rats. Behavioral neuroscience, 108(6):1196–202.

Braithwaite, S.P., Voronkov, M., Stock, J.B. & Mouradian, M.M. (2012). Targeting phosphatases as the next generation of disease modifying therapeutics for Parkinson's disease. Neurochemistry International. 61 (6): 899–906.

Brodal, P. (1992). The central nervous system: structure and function. Oxford University Press, New York.

Chassande, O., Frelin, C., Farahifar, D., Jean, T. & Lazdunski, M. (1988). The $Na^+/K^+/Cl^-$ cotransport in C6 glioma cells Properties and role in volume regulation. Eur. J. Biochem. 171,425-433.

Clementz, B. & Grampp, W. (1976). A method for rapid bevelling of micropipette electrodes. Acta Physiol. Scand. 96: 286-288.

Cohen, I., Navarro, V., Clemenceau, S., Baulac, M. & Miles, R. (2002). On the origin of interictal activity in human temporal lobe epilepsy in vitro. Science 298:1418-1421.

Coull, J. A. M., Boudreau, D., Bachand, K., Prescott, S. A., Nault, F., Sik, A., De Koninck, P. & De Koninck, Y. (2003). Trans-synaptic shift in anion gradient in spinal lamina I neurons as a mechanism of neuropathic pain. Nature Vol 424 (6951), pp. 938-42.

Crevier, D. (1993). AI: The Tumultuous Search for Artificial Intelligence, New York, NY.

Dargaeia, Z., Bangb, J. Y., Mahadevana V., Khademullaha, S., Bedarda, S., Parfitta, G. M., Kimb, J. C. & Woodina, M. A. (2018). Restoring GABAergic inhibition rescues memory deficits in a Huntington's disease mouse model. PNAS, E1618–E1626.

Deisz, R. A., Lehmann, T. N., Horn, P., Dehnicke, C. & Nitsch, R. (2011). Components of neuronal chloride transport in rat and human neocortex. J Physiol 589.6 pp. 1317–1347.

Delpire, E. (2000) Cation-Chloride Cotransporters in Neuronal Communication. News Physiol. Sci.15: 309-312.

Edman, C., Gestrelius, S. & Grampp, W. (1986). Transmembrane ion balance in slowly and rapidly adapting lobster stretch receptor neurones. J. Physiol. 377: 171-191.

Edman, C., Theander, S. & Grampp, W. (1992). Functional effects of a hyperpolarization-activated membrane current in the lobster stretch receptor neurone. Acta Physiol. Scand. 146: 221-232.

Edman, Å., Gestrelius, S. & Grampp, W. (1983). Intracellular ion control in lobster stretch receptor neurone. Acta Physiol Scand 118, 241-252.

Edman, Å., Gestrelius, S. & Grampp, W. (1987a). Analysis of gated membrane currents and mechanisms of firing control in the rapidly adapting lobster stretch receptor neurone. J Physiol 384, 649-664.

Edman, Å., Gestrelius, S. & Grampp, W. (1987b). Current activation by membrane hyper-polarization in the slowly adapting stretch receptor neurone. J Physiol 384, 671-690.

Edman, Å. & Grampp, W. (1989). Ion permeation through hyperpolarization-activated membrane channels (Q-channels) in the lobster stretch receptor neurone. Pflügers Arch 413, 249-255.

Engberg, I. (1964). Reflexes to foot muscles in the cat. Acta Physiologica Scandinavica (suppl.) 235, 1-64.

Firth, D. R. & DeFelice, J. L. (1971). Electrical resistance and volume flow in glass microelectrodes. Can. J. Physiol. Pharmacol. 49: 436-447.

Frank, M. G., Issa, N. P. & Stryker, M. P. (2001). Sleep enhances plasticity in the developing visual cortex. Neuron 30, 275–287.

Frankenhaeuser, B. & Hodgkin, A. L. (1956). The after-effects of impulses in the giant nerve fibres of Loligo. J Physiol 131, 341-376.

Fregnac, Y. & Bienenstock, E. (1998). in *Mechanistic Relationships between Development and Learning* (eds Carew, T. J., Menzel, R. & Shatz, C. J.) 113–148 (Wiley, Berlin).

Fromm M. & Schultz, S. G. (1981). Some properties of KCl filled microelectrodes: Correlation of potassium "leakage" with tip resistance. J. Membr. Biol. 62: 239-244.

Fåhraeus, C. & Grampp, W. (1993). Submembrane Na+ turnover in an isolated nerve cell preparation. In: Abstracts: XXXII Congress of the International Union of Physiological Sciences, Glasgow. Abstract No. 61.4/0.

Fåhraeus, C. Holmberg, H. & Schouenborg, J. (1996). A plausible learning algorithm for the adjustment of the nociceptive withdrawal reflex. Annual Meeting of Society for Neuroscience in Washington, D.C. 22:1125, Abstract No. 445.12.

Gerencser, G. A. & Zelezna, B. (1993). Reaction sequence and molecular mass of a Cl - translocating P-type ATPase. Proc. Natl. Acad. Sci. Vol. 90, pp. 7970-7974.

Gestrelius, S. (1983). Control of impulse firing in lobster stretch receptor neurones. Acta physiologica scandinavica supplementum, 513, 1-15.

Gestrelius, S. & Grampp, W. (1983). Kinetics of the TEA and 4-AP sensitive K^+ current in the slowly adapting lobster stretch receptor neurone. Acta Physiol Scand 118, 125-134.

Gestrelius, S., Grampp, W. & Sjölin, L. (1981). Subthreshold and near-threshold membrane currents in lobster stretch receptor neurones. J. Physiol. 310: 191-203.

Geisler, C. D., Lightfoot, E. N., Schmidt, F. P. & Sy, F. (1972). Diffusion effects of liquid-filled micropipettes: A pseudobinary analysis of electrolyte leakage. IEEE Trans. Biomed. Eng. 19: 372-375.

de los Heros, P., Alessi, D.R., Gourlay, R., Campbell, D.G., Deak, M., Macartney, T.J., Kahle, K.T. & Zhang, J. (2014). The WNK-regulated SPAK/OSR1 kinases directly phosphorylate and inhibit the K^+-Cl^- co-transporters, Biochem. J. 458, 559 - 573.

Hagbarth, K. E. (1952). Excitatory and inhibitory skin areas for flexor and extensor motoneurones. Acta Physiologica Scandinavica (suppl.) 26, 1-58.

Hamill, O.P., Marty, A., Neher, E., Sakmann, B. & Sigworth, F.J. (1981). Improved patch-clamp techniques for high-resolution current recording from cells and cell-free membrane patches. Pflugers Archiv: Eur J of Physiol Vol. 391, 85-100.

Hara, M., Inoue, M., Yasukura, T., Ohnishi, S. & Inagaki, C. (1993). Spatial Diversity of Chloride Transporters in Hippocampal Neurons. Ann NY Acad Sci 707, 421-423.

Hebb, D. O. (1949). The organization of behavior: a neuropsychological theory. New York: Wiley. 335 pp.

Hodgkin, A.L. & Huxley, A.F. (1939). Action Potentials Recorded from Inside a Nerve Fibre. Nature Vol. 144 Issue 3651, p710-711.

Holmberg, H. & Schouenborg, J. (1996a). Postnatal development of the nociceptive withdrawal reflexes in the rat: a behavioural and electromyographic study. J. Physiol. (Lond.) 493, 239–252.

Holmberg, H. & Schouenborg, J. (1996b). Developmental adaptation of withdrawal reflexes to early alteration of peripheral innervation in the rat. J. Physiol. (Lond.) 495, 399–409.

Holmberg, H., Schouenborg, J., Yu, Y-B. & Weng, H. R. (1997). Developmental adaptation of rat nociceptive withdrawal reflexes after neonatal tendon transfer. J. Neurosci. 17, 2071–2078.

Isaac, J.T., Crair, M.C., Nicoll, R.A. & Malenka, R.C. (1997). Silent synapses during development of thalamocortical inputs. Neuron 18: 269-280.

Isenberg, G. (1979). Risk and advantages of using strongly beveled microelectrodes for electrophysiological studies in cardiac purkinje fibres. Pflhgers Arch. 380: 91-98.

Kahle, K.T., Khanna, A.R., Alper, S.L., Adragna, N.C., Lauf, P.K., Sun, D. & Delpire, E. (2015). K-Cl cotransporters cell volume homeostasis, and neurological disease, Trends Mol. Med. 21, 513–523.

Kalliomäki, J., Schouenborg, J. & Dickenson, A. H. (1992). Differential Effects of a Distant Noxious Stimulus on Hindlimb Nociceptive Withdrawal Reflexes in the Rat. European Journal of Neuroscience, 4, pp. 648-652.

Katz, L. C. & Shatz, C. J. (1996). Synaptic activity and the construction of cortical circuits. Science 274, 1133–1138.

Krischer, C.C. (1969a). Theoretical treatment of ohmic and rectifying properties of electrolyte filled micropipettes. Z. Naturforschg. 24b:151–5.

Krischer, C.C. (1969b). Current voltage measurements of electrolyte filled microelectrodes with ohmic and rectifying properties. Z. Naturforschg. 24b:156–61.

Lakshminarayana, N. (1984). Equations of membrane biophysics. Orlando: Academic Press.

Lauf, P. K., Bauer, J., Adragna, N. C. Fujise, H., Zade-Oppen, A. M. M., Ryo, K. H. & Delpire, E. (1992). Erythrocyte K-Cl cotransport: properties and regulation. Am J Physiol 263, C917-C932.

Lavallée, M. & Szabo, G. (1969). The effect of glass surface conductivity phenomena on the tip potential of micropipette electrodes. In Glass Microelectrodes edited by M. Lavallée, O. F. Schanne and N. C. Hébert. New York: John Wiley & Sons, Inc., p. 95-110.

Leinekugel, X., Medina, I., Khalilov, I., Ben-Ari, Y. & Khazipov, R. (1997). Ca2+ oscillations mediated by the synergistic excitatory actions of GABA$_A$ and NMDA receptors in the neonatal hippocampus. Neuron 18: 243-255.

Lømo, Terje. (1966). Frequency potentiation of excitatory synaptic activity in the dentate area of the hippocampal formation. Acta Physiologica Scandinavica. 68 (Suppl 277): 128.

Mu, X. P., Wang, H. B., Cheng, X., Yang, L., Sun, X. Y., Qu, H. L., Zhao, S. S., Zhou, Z. K., Liu, T. T., Xiao, T., Song, B., Jolkkonen, J. & Zhao, C. S. (2017). Inhibition of Nkcc1 promotes axonal growth and motor recovery in ischemic rats. Neuroscience Vol. 365, pp. 83-93.

Nabekura, J., Ueno, T., Okabe, A., Furuta, A., Iwaki, T., Shimizu-Okabe, C., Fukuda. A. & Akaike, N. (2002). Reduction of KCC2 expression and GABA$_A$ receptor-mediated excitation after in vivo axonal injury. J Neurosci 22:4412-4417.

Nardoua, R., Ben-Aria,Y. & Khalilov, I. (2009). Bumetanide, an NKCC1 Antagonist, Does Not Prevent Formation of Epileptogenic Focus but Blocks Epileptic Focus Seizures in Immature Rat Hippocampus. J. of Neurophysiology 101:6, 2878-2888.

Nardoua, R., Ferraria, D. C. & Ben-Aria,Y. (2013). Mechanisms and effects of seizures in the immature brain. Seminars in Fetal & Neonatal Medicine 18, 175-184.

Oja, E. (1982). A simplified neuron model as a principal component analyzer. J. Math. Biol. 15, 267–273.

Okada, Y., & Inouye, A. (1976). Studies of the origin of the tip potential of glass microelectrode. Biophys. Struct. Mech. 2: 31-42.

Okabe, A., Ohno, K., Toyoda, H., Yokokura, M., Sato, K. & Fukuda, A. (2002). Amygdala kindling induces upregulation of mRNA for NKCC1, a Na^+, K^+–$2Cl^-$ cotransporter, in the rat piriform cortex. Neuroscience Research 44: 225-229.

Payne, J. A. (1997) Functional characterization of the neuronal-specific K-Cl cotransporter: implications for $[K^+]_o$ regulation. Am. J. Physiol. 273 (Cell Physiol. 42): C1516–C1525.

Payne, J. A., Rivera, C., Voipio, J. & Kaila, K. (2003). Cation–chloride co-transporters in neuronal communication, development and trauma. TRENDS in Neurosciences Vol.26 pp. 199-206.

Pouget, A. & Snyder, L. H. (2000). Computational approaches to sensorimotor transformations. Nature Neurosci. 3 (Suppl.), 1192–1198.

Ronen, G. M., Penney, S. & Andrews, W. (1999). The epidemiology of clinical neonatal seizures in Newfoundland: A population-based study. J Pediatr 134:71-5

Rosenblatt, F. (1958). The perceptron: a probabilistic model for information storage and organization in the brain. Psychol. Rev. Vol. 65, pp. 386-408.

Press, W. H., Teukolsky, S. A., Vetterling, W. T. & Flannery, B. P. (1992). Numerical Recipes in FORTRAN: The Art of Scientific Computing. Cambridge: Cambridge University Press.

Rice, C. Ll, Whitehead, R. (1965). Electrokinetic flow in a narrow cylindrical capillary. J Phys Chem 69:4017–24.

Rivera, C., Voipio, J., Payne, J. A., Ruusuvuori, E., Lahtinen, H., Lamsa, K., Pirvola, U., Saarma, M. & Kaila, K. (1999). The K^+/Cl^- co-transporter KCC2 renders GABA hyperpolarizing during neuronal maturation. Nature Vol. 397, 251-55.

Rubio, R., & G. Zubieta. (1961). The variation of the electric resistance of micro-electrodes during the flow of current. Acta Physiol. Latino-Am. 11: 91-94.

Schanne O. F., LavallJe, M. Laprade, R. & Gagne, S. (1968). Electrical properties of glass microelectrodes. Proc. IEEE. 56: 1072-1082.

Schouenborg, J. & Kalliomäki, J. (1990). Functional organization of the nociceptive withdrawal reflex. I. Activation of hindlimb muscles in the rat. Exp. Brain Res. 83, 67-78.

Schouenborg, J. & Weng, H. R. (1994). Sensorimotor transformation in a spinal motor system. Exp. Brain Res. 100, 170–174.

Schouenborg, J., Holmberg, H. & Weng, H. R. (1992) Functional organization of the nociceptive withdrawal reflexes. II. Changes of excitability and receptive fields after spinalization in the rat., Exp Brain Res Vol. 90, pp. 469-78.

Schouenborg, J., Weng, H. R., Kalliomäki, J. & Holmberg, H. (1995). A survey of spinal dorsal horn neurons encoding the spatial organization of withdrawal reflexes in the rat. Exp Brain Res Vol. 106, pp. 19-27.

Sherrington, C. S. (1906). He integrative action of the nervous system. Yale University Press. New Haven.

Sherrington, C. S. (1910). Flexion-relfex of the limb, crossed reflex and reflex stepping and standing. J Physiol Vol. 40, pp. 28-121.

Smith, J. B. & Smith, L. (1987). $Na^+/K^+/Cl^-$ Cotransport in Cultured Vascular Smooth Muscle Cells: Stimulation by Angiotensin II and Calcium Ionophores, Inhibition by Cyclic AMP and Calmodulin Antagonists. J. Membrane Biol. 99, 51-63.

Smith, C. L. & Frank, E. (1987) Peripheral specification of sensory neurons transplanted to novel locations along the neuraxis. J Neurosci Vol. 7, pp. 1537-49.

Söderlind, G. (1980). DASP-3 a program for the numerical integration of partitioned stiff ODEs and differential algebraic systems. Report TRITA-NA-8008. Stockholm: Royal Institute of Technology.

Staley, K. J., Soldo B. L. & Proctor, W. R. (1995). Ionic Mechanisms of Neuronal Excitation by Inhibitory $GABA_A$ Receptors. Science, Vol. 269, No. 5226, pp. 977-981.

Taylor R. E. Appendix to Jennerik, H. P. & Gerard, R. W. (1953). Membrane potential and threshold of single muscle fibers. J Cell Comp Physiol 42: 79–102.

Towle, D. W. & Weihrauch, D. (2001). Osmoregulation by Gills of Euryhaline Crabs: Molecular Analysis of Transporters Amer. Zool., 41:770–780.

Turrigiano, G. G., Leslie, K. R., Desai, N. S., Rutherford, L. C. & Nelson, S. B. (1998). mActivity-dependent scaling of quantal amplitude in neocortical neurons. Nature 391, 892–896.

Theander, S., Fåhraeus, C. & W. Grampp. (1996). Analysis of leak current properties in the lobster stretch receptor neurone. Acta Physiol. Scand. 157, 493–509.

Theander, S. & Grampp, W. (1997). Properties of an A-current in slowly and rapidly adapting stretch receptor neurones of lobster. Prim. Sensory Neurone 2, 211–227.

Stödberg, T. et al. (2015). Mutations in SLC12A5 in epilepsy of infancy with migrating focal seizures. Nature communications 38: pp 1-9. DOI: 10.1038/ncomms9038

Wagner. S., Castel, M., Gainer, H. & Yarom, Y. (1997). GABA in the mammalian suprachiasmatic nucleus and its role in diurnal rhythmicity. Nature 387: 598–603.

Waldenström, A., Thelin, J. & Schouenborg, J. (2001). Tactile sensory input is used for the postnatal tuning of the nociceptive withdrawal reflex system. Soc. Neurosci. Abstr. 30, 1623.

Waldenström, A., Christensson, M. & Schouenborg, J. (2002). Spontaneous movements precede and overlap in time with the tuning of the nociceptive withdrawal reflex (NWR) in postnatal rats. IASP Abstr.1558, P106.

Wang, D.D. & Kriegstein, A.R. (2008). GABA regulates excitatory synapse formation in the neocortex via NMDA receptor activation. J Neurosci, 28:5547-5558.

Weng, H. R. & Schouenborg, J. (1996). Cutaneous inhibitory receptive fields of withdrawal reflexes in the decerebrate spinal rat. J Physiol Vol. 493 pp. 253-65.

Woo, N.-S., Lu, J., England, R., McClellan, R., Dufour, S., Mount, D. B., Deutch, A. Y., Lovinger, D. M. & Delpire, E. (2002). Hyperexcitability and Epilepsy Associated With Disruption of the Mouse Neuronal-Specific K–Cl Cotransporter Gene. Hipocampus 12: 258–268.

Populärvetenskaplig sammanfattning

Kloridjonen är den vanligaste anjonen (negativt laddade jonen) i kroppen. Trots detta har kloridjonens stora betydelse för en rad fenomen, inte minst i nervsystemet, först på senare år börjat uppmärksammas i forskningen, det gäller inte minst kloridjonens roll vid inlärning och generell aktivitetsnivå i nervsystemet.

När en nervcell skickar en signal vidare till en ny nervcell sker detta via synapser. Dessa kan var excitatoriska, dvs aktivera nästa nervcell, eller inhibitoriska, dvs minska på aktiviteten i nästa nervcell. Det har länge varit känt att den jon som har allra störst betydelse för hur de inhibitoriska signalerna fungerar i vårt nervsystem är kloridjonen, framför allt koncentrationen av kloridjoner inuti nervcellerna.

Om den intracellulära kloridkoncentrationen är för hög blir nervsystemet lätt överexciterat. Detta anses numera vare en av huvudorsakerna till många typer av epilepsi, men anses även vara avgörande för neuropatisk smärta (nervsmärta) som kan uppkomma efter kirurgi eller efter skador i ryggraden. Även andra sjukdomar är sedan helt nyligen associerade med en störd kloridhomeostas (kloridjämnvikt), såsom Huntingtons sjukdom, Autismspektrumsjukdomar och Parkinson sjukdom.

Lika intressant har den senaste forskningsutvecklingen varit för kloridjonens roll vid inlärning och vid utvecklingen av nervsystemet. Man har observerat att kloridjonens roll som förmedlare av inhibitoriska signaler i det färdigutvecklade nervsystemet faktiskt är det omvända i det prenatala (unga) nervsystemet. Här verkar kloridjonen istället excitatoriskt när jonkanaler som släpper igenom kloridjonen öppnas. Kloridjonerna tycks här spela en avgörande roll för att starta ett tidsbegränsat inlärningsfönster i hjärnan. Detta inlärningsfönster migrerar i nervsystemet och verkar nödvändigt för att viss typ av inlärning skall starta.

Inlärning i nervsystemet anses idag ske via modifieringar av synapsernas styrka, dvs hur starkt eller hur mycket en presynaptisk cell (cellen före synapsen) påverkar en postsynaptisk cell (cellen efter synapsen) vid en viss synaps. Hur modifieringar av synapsernas styrka äger rum har länge debatterats, och det finns med all säkerhet olika sätt för centrala nervsystemet (CNS) att åstadkomma inlärning, men den mekanism som idag är bäst studerad beskrevs teoretiskt först av Hebb (1949), och kom sen att bevisas existera i vårt nervsystem av Terje Lömo (1966). Principen kan sägas vara korrelationsbaserad, dvs om både den presynaptiska cellen och den

postsynaptiska cellen samtidigt är aktiva så sker en stärkning av synapserna mellan dessa celler.

I den här avhandlingen handlar artiklarna I-IV i bred mening om hur kloridjonen regleras och styrs i våra nervceller och artikel V om en ny inlärningsprincip för den smärtutlösta bortdragningsreflexen.

När man studerar nervceller använder man sig ofta av en teknik där man penetrerar cellen med en mycket tunn glasmikropipett. Denna mikropipett kan sedan användas för att mäta den spänning (potential) som finns över cellens membran, den ström som passerar genom cellmembranet och slutligen även för att mäta koncentrationen av olika joner som finns inuti nervcellen, tex kloridjoner. Eftersom glasmikropipetterna har en hög koncentration av kaliumkloridjoner inuti glasmikropipettskaftet, så uppkommer ett läckage av kloridjoner som kommer påverka våra kloridjonsmätningar och även påverka själva kloridjämnvikten i den nervcell som vi studerar. Artikel I och artikel II handlar därför om att förstå i kvantitativa termer precis hur mycket glasmikropipetter stör den cell de mäter på. Vi lyckas i artikel I, via försök på kärnkraftverket i Studsvik, mäta hur många kloridjoner och kaliumjoner som läcker ut ur en glasmikropipett och även, via andra försök, karaktärisera andra egenskaper som påverkar hur en glasmikropipett påverkar sitt mätobjekt (nervcellen). I artikel II utvecklar vi en teori för vad som styr glasmikropipetters egenskaper och hur man kan kvantifiera dessa egenskaper. Det visar sig att egenskaperna beror på glasmikropipetten exakta geometri den sista tiondels millimetern och hur mycket negativa ytladdningar som glaset har på sin insida. Den teori som styr beteendet är en kombination av elektrodiffusion (diffusion i ett elektriskt fält) och elekroosmos (vätskeflöde i närvaro av elektriskt laddade ytskikt). Vi visar i artikel II, för första gången, att alla klassiska egenskaper hos glasmikropipetten går att förutsäga med mycket sort noggrannhet med den teori för mikroelektroden som vi presenterar.

Genom de mätningar på och prediktioner av hur kloridjoner och kaliumjoner läcker ut ur glasmikropipetterna när vi mäter på vår nervcell kan vi i artikel III och IV utreda vilka mekanismer som är viktiga för kloridjämnvikten i våra nervceller. Det visar sig att en så kallad kotransportör, ett membranprotein som transporterar ut en kloridjon och en kaliumjon samtidigt, är avgörande för kloridjämnvikten. Under normala omständigheter transporterar denna kaliumklorid-kotransportör ut kloridjoner (och kaliumjoner) från våra nervceller och sänker på så vis kloridkoncentration. Genom en låg intracellulär kloridkoncentration så strömmar kloridjoner in i våra nervceller när en jonkanal som är genomsläppliga för kloridjoner öppnas. På så vis säkerställs att inhibitoriska synapser i nervsystemet fungerar som de ska. Genom mätningar och simuleringar visar vi också att kaliumklorid-kotransportören kan ha en annan viktig funktion i nervsystemet, nämligen att transportera in kaliumjoner (och kloridjoner) i cellerna om den

extracellulära koncentrationen av kaliumjoner stiger snabbt, tex i samband med intensiv aktivitet hos många nervceller i ett begränsat utrymme i CNS. Under dessa omständigheter kan kaliumklorid-kotransportören bidraga till att stabilisera membranets potential så att nervsystemet kan fortsätta fungera på ett adekvat vis. I annat fall kan en störning av den extracellulära kaliumkoncentrationen leda till epileptiskt anfall.

Kaliumklorid-kotransportören har också visat sig spela stor roll i volymregleringen av celler i kroppen, så att de inte sväller för mycket. Detta görs genom att transportera ut kaliumjoner och kloridjoner ur cellerna som svar på uppsvällning. På så vis följer också vatten med och cellen kan krympa igen. I nervsystemet fungerar detta inte alltid lika bra eftersom mängden intracellulära kloridjoner är mycket lägre än i andra celler (artikel III och IV). Detta är en av orsakerna till att vid vattenförgiftning är det just hjärnan som kan ta störst skada och orsaka plötslig död. I det unga nervsystemet är kaliumklorid-kotransportören inaktiv och det är orsaken till att koncentrationen av kloridjoner är hög och att inhibitoriska signaler ofta är excitatoriska under tidig utveckling. Anledningen till att kloridkoncentrationen är hög tros vara att nervcellerna på så vis försätts i ett tillstånd där etablerandet av kontakter med andra nervceller underlättas och inlärningen vid olika synapser kan starta.

I det femte arbetet (artikel V) studeras just inlärning, närmare bestämt inlärningen av den smärtutlösta bortdragningsreflexen, som uppstår vid smärtsam hudkontakt, tex kontakt med vassa objekt eller hög värme. Denna bortdragningsreflex är i själva verket väldigt sofistikerad - var du än får en smärtsam beröring svarar kroppen omedelbart med att kontrahera precis den eller de muskler som för kroppsytan bort från den smärtsamma beröringen. Motsatsen hade naturligtvis varit evolutionärt mycket ofördelaktig (och smärtsam). Detta innebär dock att ryggmärgen har förmågan att för varje punkt på den tredimensionella kroppsytan veta vilka muskler som flyttar just den hudpunkten bort från ett objekt. Hur denna transformation går till, att från en 3D yta aktivera rätt uppsättning muskler, har debatterats länge. Man vet att den smärtutlösta bortdragningsreflexen mognar ut under råttungars första veckor efter födseln. Tidigare har man ansett att detta var nedärvda egenskaper men nyligen har en serie experiment visat att detta med stor säkerhet är fel och att reflexen istället är inlärd. Man har tex visat att varje muskel verkar ha ett hudområde den aktiveras från om hudytan utsätts för smärta. Man har också visat att om muskelns senfäste flyttas, så att muskeln utför en ny rörelse av hudytan, så flyttas också det hudområde som muskeln aktiveras från vid smärtsam beröring. En annan intressant observation är att den smärtutlösta reflexen mognar ut även om man tar bort all smärtsam stimulus under utvecklingsperioden. Tar man bort övrig (taktil) känsel så mognar dock inte reflexen ut på korrekt vis.

Baserat på denna information konstruerades en matematisk modell över ryggmärgen med följande egenskaper. Spontanaktiva nervceller i ryggmärgen, kanske spontanaktiva på grund av hög intracellulär kloridjonskoncentration, aktiverar en muskel åt gången, precis som fosterrörelser hos människor eller muskeltwitchar hos nyfödda råttungar. När muskeln aktiveras så avlastas en hudyta och denna taktila (känsel) information skickas tillbaka till ryggmärgen där den sammanstrålar med smärtinformation från samma hudområde. I nästa steg sprids denna information till alla nervceller i ryggmärgen som ingår i denna nervkrets. Den nervcell som var aktiv i att skicka signalen, kan då korrelera sin aktivitet med den inkommande signalen, och på så vis lära sig genom att stärka den synaps som är associerad med den hudyta muskeln påverkade vid sin sammandragning. Möjligen lärs alla reflexer in på ett liknande vis, genom att nervsystemet alstrar testsignaler som sedan kommer tillbaka som sensorisk feedback efter muskelns sammandragning. Man kan också tänka sig att testpulser är viktiga i andra delar av nervsystemet för att utreda hur en nervkrets hänger samman och att detta därför är en, av flera, generella principer för hur nervsystemet mognar ut till den formidabla maskin det är hos vuxna individer.

Acknowledgement

Among all the people, that I had the opportunity to work and interact with during the completion of this thesis, there are many to whom I am particularly grateful:

My late supervisor, professor **Wolfgang Grampp**, one of the wisest men I have met, who told me many things, not only in science, worth remembering and contemplating;

Gudrun Grampp, for wonderful hospitality and many interesting stories when you hosted dinners;

Henrik Jörntell, for a remarkable kindness, attentiveness and knowledge in all aspects I could asked for - neuroscience issues, faculty politics or practical things such as deadlines for printing the dissertation;

Jens Schouenborg for a stringent calm and for allowing me to play with his data in constructing the mathematical model for the learning of the nociceptive withdrawal reflex;

My PhD friends **Kalle Swärd, Maria Gomez, Martin Garwisz, Mark Kornfeld, Hans Holmberg and Henrik Jörntell** from back then at the Dept of Physiology, when I was a fulltime PhD student, for all the fun memories. And it is fantastic to see that you all have accomplished so much since;

My PhD colleagues, sharing Wolfgang Grampp as supervising professor, **Sten Theander** and **Staffan Skogvall,** for exciting discussions and one or two refreshing disagreements;

The staff at the Department of Physiology, **Olle Hammar, Martin Nyström, Daniel Rubensson**, **Mats Wokander, Åke Sigurdh** and **Leif Nilsson** for providing the general and specialized tools without which no research could have been done and also for helping me with enigmatic computer issues;

Kristina Borglid, for excellent technical support, and for great friendliness and warmth, and not the least for the skilled contribution as co-author in Paper I;

Professor **Carsten Peterson**, for introducing me to artificial neural networks, and discussing ANN learning strategies with me in the early days of my PhD;